Structural Changes during the Formation of Early Intermediates in the Bacteriorhodopsin Photocycle

Shigehiko Hayashi, Emad Tajkhorshid, and Klaus Schulten
Beckman Institute, University of Illinois at Urbana-Champaign, Urbana, Illinois 61801 USA

ABSTRACT Early intermediates of bacteriorhodopsin's photocycle were modeled by means of ab initio quantum mechanical/molecular mechanical and molecular dynamics simulations. The photoisomerization of the retinal chromophore and the formation of photoproducts corresponding to the early intermediates were simulated by molecular dynamics simulations. By means of the quantum mechanical/molecular mechanical method, the resulting structures were refined and the respective excitation energies were calculated. Two sequential intermediates were found with absorption maxima that exhibit red shifts from the resting state. The intermediates were therefore assigned to the K and KL states. In K, the conformation of the retinal chromophore is strongly deformed, and the N—H bond of the Schiff base points almost perpendicular to the membrane normal toward Asp-212. The strongly deformed conformation of the chromophore and weakened interaction of the Schiff base with the surrounding polar groups are the means by which the absorbed energy is stored. During the K-to-KL transition, the chromophore undergoes further conformational changes that result in the formation of a hydrogen bond between the N—H group of the Schiff base and Thr-89 as well as other rearrangements of the hydrogen-bond network in the vicinity of the Schiff base, which are suggested to play a key role in the proton transfer process in the later phase of the photocycle.

INTRODUCTION

Bacteriorhodopsin (bR), a transmembrane protein residing in the purple membrane of *Halobacterium salinarum*, functions as a light-driven proton pump to produce a proton gradient across the membrane (Oesterhelt and Stoeckenius, 1971). The protein consists of seven transmembrane α-helices (Henderson and Unwin, 1975) surrounding an all-*trans* retinal chromophore covalently bound to Lys-216 through a protonated Schiff base linkage. Fig. 1 depicts the chemical structure of the protonated all-*trans* retinal Schiff base and its link to the protein. Retinal contains six conjugated double bonds including the Schiff base group.

Upon absorption of light in the visible spectral region, the retinal chromophore undergoes in bR an isomerization around the $C_{13}{=}C_{14}$ double bond, resulting in a 13-*cis* configuration. The photoisomerization initiates a photocycle during which bR completes an active proton transport event across the membrane from cytoplasm to the extracellular side. The photocycle comprises a series of intermediates, labeled K, L, M, N, and O, characterized by their absorption maxima, and is completed through return to the initial (BR) state (Lozier et al., 1975). The lifetimes of the intermediates range from subpicoseconds to milliseconds. The photocycle involves protein structural changes, which are coupled to proton transfer between such key residues as the retinal Schiff base, Asp-85, Asp-96, and Glu-204 (Braiman et al., 1988; Gerwert et al., 1989; Brown et al., 1995). A sequence of proton transfers between these residues completes the overall unidirectional proton pump through the channel.

The three-dimensional atomic structure of the resting BR state has been determined by cryoelectronic microscopy (Grigorieff et al., 1996; Mitsuoka et al., 1999) and x-ray crystallography (Pebay-Peyroula et al., 1997; Luecke et al., 1998, 1999a,b; Belrhali et al., 1999). These structures reveal the position of key residues facing the interior of the protein and forming the proton channel. The protonated Schiff base group lies in the middle of the channel dividing it into the cytoplasmic and extracellular half-channels. High resolution x-ray structures (Luecke et al., 1999a; Belrhali et al., 1999) have also shown a hydrogen-bond network (HBN) in the extracellular half of the channel including several internal water molecules. The existence of water molecules was first suggested by nuclear magnetic resonance (NMR) (de Groot et al., 1989) and Fourier transform infrared (FTIR) spectroscopic studies (Maeda et al., 1994; Fischer et al., 1994; Kandori et al., 1995; Chon et al., 1996). In Fig. 2 *a*, the structure of the retinal binding site of the x-ray structure of BR (Luecke et al., 1999a; PDB code, 1C3W) is shown. Fig. 3 illustrates the topology of the HBN in the retinal binding pocket, including the negatively charged Asp-85 and Asp-212, the Schiff base, and three internal water molecules (Wat-401, Wat-402, and Wat-406).

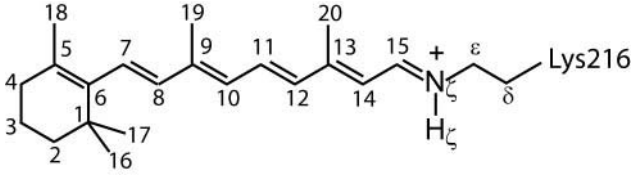

FIGURE 1 Schematic representation of all-*trans* retinal bound via a protonated Schiff base to Lys-216 in bR and its conventional atom numbering.

Submitted January 11, 2002, and accepted for publication May 7, 2002.

Address reprint requests to Klaus Schulten, 405 N. Mathews Avenue, Urbana, IL 61801. Tel.: 217-244-1604; Fax: 217-244-6078; E-mail: KSchulte@ks.uiuc.edu.

0006-3495/02/09/1281/17 $2.00

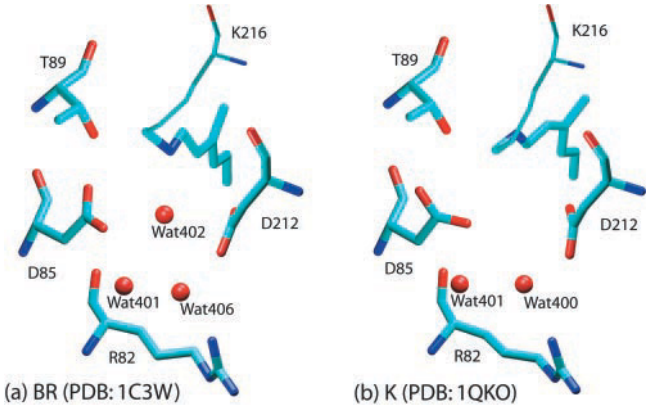

FIGURE 2 Comparison of the x-ray crystallographic structures in the vicinity of the Schiff base in (*a*) BR (Luecke et al., 1999a; PDB, 1C3W) and (*b*) K (Edman et al., 1999; PDB, 1QKO) states. The β-ionone halves of the chromophore are not shown. In the structure of the K intermediate, dislocation of Wat-402 and rotation of the carboxyl group of Asp-85 are observed. Wat-400 in the K model of Edman et al. (1999) corresponds to Wat-406 in the model of BR of Luecke et al. (1999a).

After photoisomerization, a bathochromic (red-shifted) intermediate, called K, forms in 3 ps. The K state that is trapped at liquid nitrogen temperature 77 K is called K_{LT}. In K, the energy of the absorbed photon is stored in a high energy structure, the relaxation of which induces a controlled series of proton translocations. The stored energy has been estimated to be 16 kcal/mol by photocalorimetric experiments (Birge and Cooper, 1983; Birge et al., 1989). The structural changes during the K formation have been extensively investigated by various methods. Low temperature resonance Raman (LT-RR) and low temperature FTIR (LT-FTIR) spectroscopic studies have shown significant chromophore conformational deformations in K_{LT} (Pande et al., 1981; Braiman and Mathies, 1982; Bagley et al., 1982; Rothschild and Marrero, 1982). LT-FTIR studies have also revealed alterations of the HBN in the vicinity of the Schiff base during the K formation (Kandori et al., 1998a,b, 1999, 2000, 2001a; Kandori and Shichida, 2000).

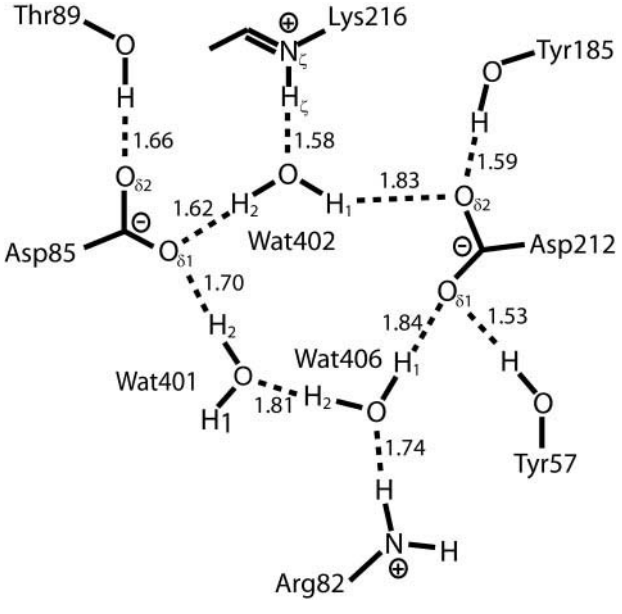

FIGURE 3 Schematic representation of the hydrogen-bond network in the binding pocket in the BR state and atom numbering used in the text. Dashed lines indicates possible hydrogen bonds. Distances of the hydrogen bonds are shown in Å.

Recently, an x-ray crystallographic structural model of the K_{LT} intermediate has been reported (Edman et al., 1999). Fig. 2 *b* shows the retinal binding site of the x-ray structure (PDB code, 1QKO). The K—BR difference electron density map reported in that study (Edman et al., 1999) clearly shows a strong negative density at the position of Wat-402 in BR, indicating the dislocation of this water molecule during the formation of K_{LT}. The density map also reveals a remarkable conformational change of Asp-85, which leads to the complete dissociation of its hydrogen bond with Thr-89 and its closer distance to the Schiff base. The authors have argued that these structural changes play a key role in the primary proton transfer between the Schiff base and Asp-85 in a later (L-to-M) step. However, due to the weak electron density for K_{LT}, the position of the dislocated W-402 and the conformation of the chromophore in K_{LT} have not been determined clearly. Moreover, the complete dissociation of the hydrogen bond between Asp-85 and Thr-89 disagrees with recent LT-FTIR results that indicate a stronger hydrogen bond between these groups upon the formation of K_{LT} (Kandori et al., 1998b, 1999, 2001).

Two distinct K-like bathochromic intermediates have been resolved by visible (Shichida et al., 1983), FTIR (Rothschild et al., 1985; Sasaki et al., 1993; Weidlich and Siebert, 1993; Hage et al., 1996; Dioumaev and Braiman, 1997), and resonance Raman (Althaus et al., 1995; Doig et al., 1991) spectroscopic measurements. These intermediates appear sequentially in time, and the early and late ones have been conventionally called K and KL, respectively. The formation of KL at room temperature has been observed in ~10 ns by the visible absorption measurements (Shichida et al., 1983), and in 50 to 100 ns by the time resolved FTIR (TR-FTIR) experiments (Hage et al., 1996; Dioumaev and Braiman, 1997). Although the spectroscopic studies have suggested significant structural changes involved in the K-to-KL transition, the KL intermediate has not been well understood at the atomic level.

The structure and dynamics of bR have been investigated by many theoretical studies (Schulten et al., 1995; Logunov and Schulten, 1996; Xu et al., 1996; Humphrey et al., 1998; Ben-nun et al., 1998; Tajkhorshid et al., 2000; Baudry et al., 2001; Warshel et al., 1991; Warshel and Chu, 2001; Nina et al., 1995; Yamato and Kakitani, 1997). Recently, ab initio quantum mechanical/molecular mechanical (QM/MM) calculations have been applied to investigate the structure, the

proton transfer reaction, and the electronic and vibrational absorptions of the BR state (Hayashi and Ohmine, 2000).

QM/MM methods have been widely used to study chemical reactions in solution phase and in proteins (Warshel and Levitt, 1976; Warshel et al., 1991; Warshel and Chu, 2001; Field et al., 1990; Gogonea et al., 2001; Maseras and Morokuma, 1995; Merill and Gordon, 1998; Gao and Xia, 1992; Logunov and Schulten, 1996). In QM/MM methods, the part of the system that involves electronic changes is described quantum mechanically (QM), and the rest, which provides steric and electrostatic environmental effects on the QM part, is treated by a molecular mechanical (MM) force field.

Hayashi and Ohmine (2000) computed the proton transfer potential energy profile in bR by QM/MM calculations and showed that the primary proton transfer can be efficiently triggered by a certain rearrangement of the HBN, which can be induced by the chromophore photoisomerization (Hayashi and Ohmine, 2000). The authors have also described quantum mechanically the electronic structures of the chromophore and the HBN in the vicinity of the Schiff base, which is closely involved in the proton transfer process. The electronic nature of the HBN results in anomalous IR signals of the O—D and N—D stretching modes that have been confirmed by a recent IR measurement (Kandori et al., 2002). The excitation energy of the chromophore in the protein matrix was also calculated and analyzed in terms of the chromophore-protein interactions. The ab initio QM/MM approach has also been applied to identify the molecular mechanism of prominent absorption spectral features of sensory rhodopsin II (Hayashi et al., 2001), for which x-ray crystallographic structures have been determined recently (Royant et al., 2001; Luecke et al., 2001).

In the present paper, we report molecular dynamics (MD) simulations and ab initio QM/MM calculations modeling the early intermediates of bR's photocycle. The photoisomerization and the formation of the photoproducts, i.e., the early intermediates, were simulated by MD. As mentioned above, a proper description of electronic effects of the chromophore and the HBN is crucial for the study of the chromophore-protein interactions and their dynamics. Thus, we introduce a polarizable water model (Rick et al., 1994) for internal water molecules and reparameterized the force field functions by the QM/MM method. The structures of the photoproducts obtained by MD simulations are further refined by QM/MM full geometry optimizations, where the chromophore and the HBN are calculated fully quantum mechanically. At the optimized structures of the intermediates, electronic excitation energies of the chromophore were also calculated to characterize the identified intermediates and to elucidate the molecular basis of their bathochromic shifts. The present study provides detailed atomic structural models of the K and KL intermediates and suggests key structural changes in the proton pump process. The study also addresses discrepancies between the x-ray structural model and spectroscopic observations.

METHODS

In this section, details of preparation of the structural model will be first presented. Then, we will describe protocols and potential energy functions used for MD simulation of the chromophore isomerization and the formation of intermediates. Finally, methods of the QM/MM geometry optimization, energy decomposition analysis, and excitation energy calculations will be described.

Structural model

A structural model of the ground state (BR) was constructed based on the high resolution crystal structures (Luecke et al., 1999a; Belrhali et al., 1999). The model includes nine water molecules: two in the cytoplasmic half of the channel, three in the Schiff base binding site (Wat-401, Wat-402, and Wat-406), one between Arg-82 and Thr-205, and three in the vicinity of Glu-194 and Glu-204. Asp-96, Asp-115, and Glu-204 were protonated, and the other acidic and basic residues were assumed to be charged (Sasaki et al., 1994; Brown et al., 1995).

MD simulation

MD simulations were used to model the chromophore photoisomerization and to obtain starting structural models of the early intermediates, which were refined by the QM/MM optimization described in the next section. The AMBER force field (Cornell et al., 1995) was used for the standard protein residues, whereas force fields of the retinal chromophore and water molecules were reparameterized based on the QM/MM methods, as described below. Time integration of the equation of motion was performed by the leap-frog algorithm with a 1-fs time step. The bond distances including hydrogen atoms were kept fixed by SHAKE. To maintain the overall shape of the protein, harmonic constraints with a force constant of 2.0 kcal/mol/Å^2 were applied to C_α atoms further than 12 Å from the retinal chromophore. This approximation is validated by electron microscopic (Bullough and Henderson, 1999) and x-ray crystallographic (Edman et al., 1999) studies, showing that no major conformational changes of helices accompany the formation of K. A 12-Å residue-based cutoff was used for nonbonding interactions. The Berendsen method (Berendsen et al., 1984) was used to control the temperature.

The BR ground state was equilibrated for 200 ps at 300 K starting from the QM/MM optimized structure (Hayashi and Ohmine, 2000), and then an equilibrium simulation of BR for 300 ps was performed to sample initial coordinates and velocities for the simulations of photoisomerization. The chromophore photoisomerization was simulated from the initial configurations using the potential energy function of the excited state, which steers the 13-*trans* excited state to the 13-*cis* ground state photoproduct (see below). During the isomerization, the temperature control was turned off. To determine energy minimized structures of the photoproducts from trajectories of the photoisomerization, the system was first cooled gradually to 50 K in 40 ps and then subjected to the QM/MM optimization.

For the BR ground state, we used the force field parameters of dihedral angles of the main polyene chain of retinal (set B in Tajkhorshid et al., 2000) determined previously based on density functional calculations (Tajkhorshid et al., 1999). In addition, improper torsional functions with $V_n/2 = 0.3$ kcal/mol were applied to represent sp^2 planarities in the conjugated polyene.

For the isomerization, the potential energy function of the C_{13}═C_{14} dihedral angle, $\phi_{13=14}$, was expressed by seven Fourier components listed in Table 1. Fig. 4 shows the energy profile of the potential function. The internal conversion to the 13-*cis* ground state is described by downhill dynamics on a single potential curve. In this description, the electronic details of the transition process from the excited state to the ground state during the isomerization are neglected. We assumed that the reactive trajectories to the 13-*cis* configurations are not drastically perturbed by the

TABLE 1 Force field parameters for the C_{12}—C_{13}═C_{14}—C_{15} torsional coordinate of protonated retinal Schiff base in the S_1 excited state*

n	$V_n/2^\dagger$	$\gamma^\ddagger$
1	20.26	180.0
2	−6.80	0.0
3	−0.79	180.0
4	0.33	0.0
5	0.11	180.0
6	−0.04	0.0
7	−0.02	180.0

*Potential energy for the torsion is expressed as $\Sigma_n(V_n/2)(1 + \cos(n\phi_{13=14} - \gamma))$, in which $\phi_{13=14}$ is the dihedral angle.
†Values are in kcal/mol.
‡Values are in degree.

electronic transition process, because the internal conversion likely takes place through conical intersections, which are expected to be highly efficient doorways to the ground state. The potential energy curve displays a plateau region around the 13-*trans* configuration, as suggested by quantum chemical calculations (Garavelli et al., 1997, 1998; Humphrey et al., 1998; González-Luque et al., 2000). Unfortunately, the accurate excited state potential profile of the chromophore with six double bonds in the protein matrix has not been calculated yet. We therefore repeated the photoisomerization with several trial potential functions that differ with respect to the width of the plateau region. Those different potential functions produced almost the same photoproducts, although the isomerization rate was sensitive to the width. The other dihedral parameters of the chromophore remained the same as those in the ground state, except for C_{15}═N_ζ and C_{14}—C_{15}, for which we used single well potentials with the same curvatures at the *trans* configurations to inhibit their rotations.

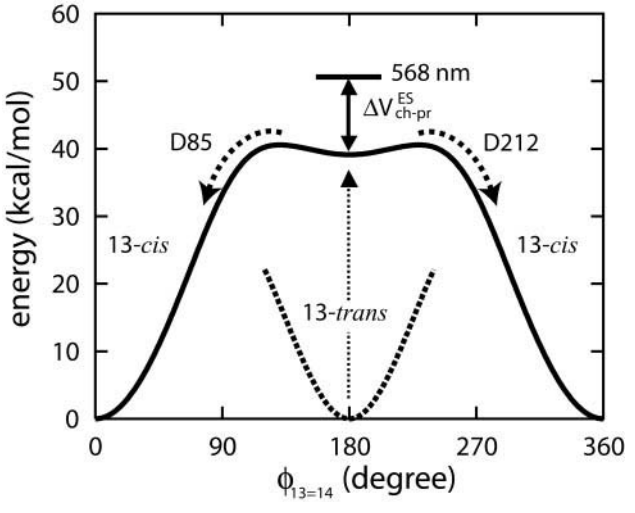

FIGURE 4 Energy profile of the potential function of the C_{13}═C_{14} dihedral coordinate, $\phi_{13=14}$, of the retinal chromophore used in the MD simulations of the photoisomerization. In the electronical ground state, the dihedral potential energy function possesses a minimum at the 13-*trans* configuration, represented by a dashed line. At the time photoabsorption takes place, the potential function is switched to the reactive one, represented by a solid line, which leads to the isomerization to the 13-*cis* configuration. There are two possible directions of the isomerization, rotation of the N—H bond of the Schiff base toward Asp-85 or toward Asp-212, because the dihedral potential function is symmetric. The vertical energy difference of the dihedral potential functions at the planar 13-*trans* configuration is set to be 39.1 kcal/mol, which together with the contribution from the chromophore-protein electrostatic interaction, $\Delta V^{ES}_{ch—pr} = 11.2$ kcal/mol, reproduces the experimental absorption energy (50.3 kcal/mol).

Recently, the reaction potential energy surfaces of retinal analogues from the Franck-Condon region to the product state in isolated form have been precisely investigated by means of high-level quantum chemical calculations (Garavelli et al., 1997, 1998; Humphrey et al., 1998; González-Luque et al., 2000; Molnar et al., 2000). These studies showed the involvement of the stretching motions of the polyene skeleton in the isomerization process, especially in the initial 100 to 200 fs (the H-to-I process) and during the electronic transition at the conical intersections. The quantum dynamics of the electronic transitions in the protein matrix has also been examined by semiclassical techniques (Humphrey et al., 1998; Ben-nun et al., 1998; Warshel and Chu, 2001), suggesting mechanisms accounting for the high quantum yield (0.64) of the isomerization process in bR. The present classical treatment of the isomerization by a one-dimensional potential function is a rather crude approximation and unable to reproduce prominent characteristics of the photoisomerization dynamics observed in ultrafast spectroscopic studies. Nevertheless, it seems to be unlikely that lack of the details of the actual photodynamics leads to a qualitatively irrelevant structural model of the primary photoproduct, because the conformational change of the chromophore during the isomerization is apparently dominated by the rotation around the C_{13}═C_{14} bond. Moreover, the quality of the structures of the photoproducts, which may be compromised by the applied simple potential functions of the chromophore, is improved through the QM/MM structure refinements that follow the MD simulations in the present modeling scheme.

It is well known that the charge distribution of the retinal chromophore in bR largely changes both during the photoexcitation and isomerization. Therefore, we used effective charge parameters for the chromophore in the ground and excited states, $q_i^{S_0}$ and $q_i^{S_1}$, respectively, derived from QM/MM complete active space self-consistent field (CASSCF) calculations performed at the ground state energy minimum geometry (Hayashi et al., 2001). These charges are listed in Table 2. The change of charge distribution during the isomerization was then expressed by a function that analytically interpolates $q_i^{S_0}$ and $q_i^{S_1}$ smoothly at $\phi_{13=14} = 90°$ and 270°,

$$q_i = q_i^{S_0} \times \frac{1}{2}(1 - \tanh \Phi) + q_i^{S_1} \times \frac{1}{2}(1 + \tanh \Phi), \quad (1)$$

$$\Phi = \frac{-|180 - \phi_{13=14}| + 90}{a \times 90}. \quad (2)$$

a was chosen to be 0.1, which gives an abrupt switch of the charges around $\phi_{13=14} = 90°$ and 270° to mimic the so-called sudden polarization at the conical intersection. It is noted that the change of the charge distribution upon the excitation results in a difference of the chromophore-protein electrostatic interactions, $\Delta V^{ES}_{ch—pr}$ and, therefore, contributes to the S_1—S_0 excitation energy (see QM/MM excitation energy calculations section). In the BR state, the $\Delta V^{ES}_{ch—pr}$ contribution for this effective charge parameter set was estimated to be 11.2 kcal/mol by our preliminary MD simulations. Therefore, the vertical energy difference of the internal potential functions at $\phi_{13=14} = 180°$ was set to be 39.1 kcal/mol (=50.3 kcal/mol (568 nm) − 11.2 kcal/mol) as shown in Fig. 4.

Rearrangement of the HBN in the proton channel plays an important role for the pump process. Therefore, a proper description of the HBN is also crucial in our MD simulation. As shown by a previous QM/MM study (Hayashi and Ohmine, 2000), there are strong electronic interactions, such as polarization and charge transfer, between the Schiff base, Asp-85, and Wat-402. The Kitaura-Morokuma energy decomposition analysis (Kitaura and Morokuma, 1976) showed that Wat-402 has a polarization energy of −14.1 kcal/mol and a charge transfer energy of −18.2 kcal/mol due to its interaction with the Schiff base, Asp-85, and other surrounding moieties.

TABLE 2 RESP atomic charges* of the chromophore in the ground (S_0) and excited (S_1) states

Atom	S_0	S_1	Atom	S_0	S_1	Atom	S_0	S_1
C_γ	−0.1115	−0.1157	C_{11}	−0.0439	−0.0704	C_2	0.0033	0.0040
H_γ	0.0279	0.0282	H_{11}	0.1394	0.0852	H_2	0.0086	0.0101
C_δ	0.0178	0.0271	C_{10}	−0.1435	−0.0816	C_1	0.0094	0.0148
H_δ	0.0256	0.0250	H_{10}	0.1252	0.1517	C_{20}	−0.0004	−0.0038
C_ε	0.0407	0.0153	C_9	−0.1179	−0.0743	H_{20}	0.0440	0.0385
H_ε	0.0665	0.0702	C_8	−0.0951	−0.0461	C_{19}	−0.0006	−0.0008
N_ζ	−0.0601	−0.1453	H_8	0.0823	0.0857	H_{19}	0.0625	0.0605
H_ζ	0.4037	0.4031	C_7	−0.0665	−0.0392	C_{18}	0.0046	0.0059
C_{15}	−0.0881	−0.2014	H_7	−0.0058	−0.0016	H_{18}	0.0138	0.0135
H_{15}	0.2646	0.2401	C_6	−0.0337	−0.0011	C_{17}	−0.0139	−0.0172
C_{14}	−0.1780	−0.1618	C_5	0.0260	0.0757	H_{17}	−0.0005	0.0006
H_{14}	0.1401	0.1625	C_4	0.0031	0.0061	C_{16}	−0.0261	−0.0295
C_{13}	0.0043	−0.0595	H_4	0.0206	0.0230	H_{16}	0.0020	0.0014
C_{12}	−0.1661	−0.1233	C_3	0.0167	0.0239			
H_{12}	0.1869	0.2009	H_3	−0.0089	−0.0115			

*Restrained electrostatic potential derived charges (Bayly et al., 1993).

These electronic interaction energies are considerably larger than those in water-water interactions; for example, the polarization and charge transfer energies in a water dimer are approximately −1 to −2 kcal/mol (Umeyama and Morokuma, 1977). In our preliminary MD simulations, we found that the TIP3P-AMBER force field, in which nonbonding interactions are described by only classical pair-wise potential functions, cannot even reproduce the conformation of Wat-402 observed in the x-ray ground state structure; after the MD equilibration, the Schiff base N—H bond directly attaches to O_{δ_2} of Asp-85, and Wat-402 no longer bridges the two. We also observed in the QM/MM optimized ground state structure a strong interaction between N—H of the Schiff base and a lone pair orbital of Wat-402 (Hayashi and Ohmine, 2000); the TIP3P water model cannot represent this hydrogen-bond correctly because of the poor description of the lone pairs and electronic interactions.

Fig. 5 compares the interaction energies of Wat-402 with its surroundings in bR, determined in the frame work of the TIP3P-AMBER force field, or by means of the QM/MM calculations. Details of the QM/MM calculations are described in the next section. The energies were estimated for the energy minimum conformation and for 26 other conformations generated by ±15° rotations of the Wat-402 molecule around the Cartesian axes. As clearly seen, the TIP3P-AMBER energies strongly deviate from the QM/MM ones, indicating the poor orientational description of the TIP3P model due to lack of lone pair electrons and electronic interactions.

The potential functions describing the internal water molecules were therefore improved as follows. First, the fluctuating charge model (fq-SPC) developed by Rick et al. (1994) was used for all water molecules. This model can take into account the multibody effect due to the electronic polarization induced by the polar environment. Furthermore, we added potential energy terms representing explicitly the angular dependence of hydrogen-bonds and short-range attractions between Wat-402 and the counter-ion aspartate groups. Parameters appearing in the additional potential energy terms were fitted so as to reproduce the QM/MM energies. The reparameterized force field is denoted as set 1. The functional forms and parameters are summarized in an Appendix. Fig. 5 also compares the interaction energies of Wat-402 by using the set 1 force field with the QM/MM values. One can see that the energies of the present model are in good agreement with those of the QM/MM results. Using this model for water, the hydrogen-bond network of the ground state remained stable during a 500-ps MD trajectory. In the simulations of photoisomerization, these additional functions were excluded for the excited state and smoothly switched on during the isomerization with the same switching function used for effective charges (see Eqs. 1 and 2). In the simulations for the modeling of KL, we used the fq-SPC model for Wat-402 but removed the additional functions (see the KL intermediate section). This force field is denoted as set 2.

QM/MM geometry optimization

The early intermediate structures obtained by the MD simulations were refined through QM/MM geometry optimizations. We used a QM/MM method described elsewhere (Hayashi and Ohmine, 2000) that allows one to determine efficiently the optimized geometry of the whole system. One-electron operators based on a restrained electrostatic potential (RESP) method (Bayly et al., 1993) were used to describe the electrostatic interaction between the QM and MM regions, thus, avoiding the time consuming computation of electron integrals of gradient components due to the QM—MM interaction during the optimization of the MM region, which usually needs a large number of searching steps. The QM/MM method is implemented in the HONDO (Dupuis et al., 1994) program package. The AMBER force field (Cornell et al., 1995) and the Hartree-Fock (HF) level of theory were used for the description of the MM and QM regions,

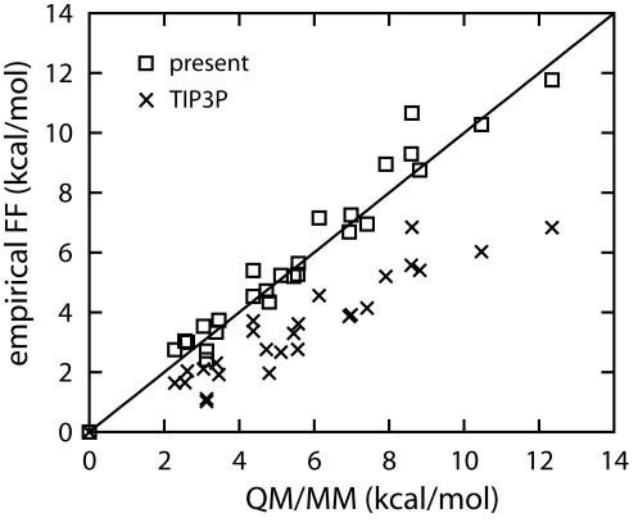

FIGURE 5 Comparison of the interaction energies of Wat-402 with its surroundings, obtained by different empirical force field functions with those obtained by means of the QM/MM method. The energies were evaluated at 27 conformations that were generated by changing orientation of the Wat-402 molecule from the energy minimum geometry. × and □ indicate results of the TIP3P and set 1 models (MD simulation section), respectively.

respectively. For the geometry optimization, the side chains of retinal-Lys-216, Asp-85, and Asp-212, as well as three water molecules (Wat-401, Wat-402, and Wat-406) were included in the QM part. Dunning's split-valence (DZV) basis set (Dunning and Hay, 1977) was used together with diffuse functions on the O_δ atoms of the aspartate side chains. The boundaries dividing the QM and MM regions were set at the C_β—C_γ bond of Lys-216 and the C_α—C_β bonds of Asp-85 and Asp-212, and the open valences in the QM region were filled by dummy hydrogen atoms following the link atom approach (Field et al., 1990). The interactions between the dummy hydrogen atoms and the MM region were excluded by the RESP treatment (Hayashi and Ohmine, 2000). A 12-Å residue-based cutoff was used for nonbonding interactions.

QM/MM energy decomposition analysis

The QM/MM energies of the BR and intermediate states were analyzed by decomposing them into several contributions. The total energy of the QM/MM system is expressed as

$$E = E_{\mathrm{QM/MM}} + E_{\mathrm{MM}}, \tag{3}$$

in which $E_{\mathrm{QM/MM}}$ includes energies of the QM region itself and of the QM—MM interaction, and E_{MM} consists of only interactions within the MM region. Unfortunately, it is rather difficult to consistently determine E_{MM} of different states in the present scheme because of large fluctuations of polar residues around the surface regions. In this study, therefore, we examined only the $E_{\mathrm{QM/MM}}$ term.

$E_{\mathrm{QM/MM}}$ is decomposed into several terms:

$$E_{\mathrm{QM/MM}} = E^0 + V^{\mathrm{ES}}_{\mathrm{QM—MM}} + V^{\mathrm{LJ}}_{\mathrm{QM—MM}} + V^{\mathrm{BAD}}_{\mathrm{QM—MM}} + E^{\mathrm{ERO}}_{\mathrm{QM(MM)}}. \tag{4}$$

E^0 is the QM energy in isolated condition computed at the geometry inside the protein matrix. $V^{\mathrm{ES}}_{\mathrm{QM—MM}}$ and $V^{\mathrm{LJ}}_{\mathrm{QM—MM}}$ are electrostatic and Lennard-Jones (LJ) interactions between the QM and MM regions, respectively. $V^{\mathrm{BAD}}_{\mathrm{QM—MM}}$ expresses the bonding contributions (bond, angle, and dihedral) at the QM/MM boundary. $E^{\mathrm{ERO}}_{\mathrm{QM(MM)}}$ is the electronic reorganization (ERO) energy. The external electrostatic field produced by the MM protein matrix polarizes the QM electronic wave function and naturally contributes to $\Delta V^{\mathrm{ES}}_{\mathrm{QM—MM}}$. The induced polarization, however, involves deformation of the electronic wave function, known as ERO, and therefore gives rise to a destabilization effect that to some extent compensates the electrostatic stabilizations (Gao and Xia, 1992; Gao, 1997).

We carried out this analysis for the same QM/MM system used in the geometry optimizations. The QM region includes side chains of retinal-Lys-216, Asp-85, and Asp-212, and three water molecules (see QM/MM geometry optimization section). This QM/MM system is denoted as system A. We also applied the analysis to a QM/MM system in which only the side chain of retinal-Lys-216 is included in the QM region, denoted as system B. In both systems, the QM regions were described by the HF method with the DZV basis set.

QM/MM excitation energy calculations

In the description of the excited state, we employed the QM/MM method using the CASSCF level of theory. The excitation energy (E_{ex}) was computed for system B (see QM/MM energy decomposition analysis section). Twelve electrons in 11 valence π orbitals of the chromophore were chosen for the CAS space. To improve the flexibility of basis functions, polarization functions were added to the C and N atoms of the conjugated backbone of the retinal Schiff base. The excitation energies were computed by the state-averaged CASSCF calculations for the lowest three π-π^* states (S_0, S_1, and S_2), followed by the state specific CASSCF calculations for the S_0 and S_1 states.

To analyze the molecular mechanism of the characteristic bathochromic shifts of the intermediates, E_{ex} was also decomposed in the same way as described in QM/MM energy decomposition analysis section. Because $V^{\mathrm{LJ}}_{\mathrm{QM—MM}}$ and $V^{\mathrm{BAD}}_{\mathrm{QM—MM}}$ do not change upon the excitations, E_{ex} is expressed by only three contributions (Hayashi et al., 2001),

$$E_{\mathrm{ex}} = E^0_{\mathrm{ex}} + \Delta V^{\mathrm{ES}}_{\mathrm{ch—pr}} + \Delta E^{\mathrm{ERO}}_{\mathrm{ch(pr)}}. \tag{5}$$

Here E^0_{ex} is the excitation energy in isolated condition; $\Delta V^{\mathrm{ES}}_{\mathrm{ch—pr}}$ is the difference between the chromophore(ch)-protein(pr) electrostatic interaction energies in the S_0 and S_1 states; $\Delta E^{\mathrm{ERO}}_{\mathrm{ch(pr)}}$ is the difference between the ERO energies in those states. Note that upon excitation the positive charge of the chromophore, which is mainly localized in the Schiff base region in the ground state, migrates toward the β-ionone ring side of the polyene chain. Hence, the negatively charged counter-ion groups in the vicinity of the Schiff base stabilize the ground state more strongly than the excited state, and, consequently, $\Delta V^{\mathrm{ES}}_{\mathrm{ch—pr}}$ is a large positive contribution (Hayashi and Ohmine, 2000; Hayashi et al., 2001).

RESULTS

MD simulations were performed to examine the photoisomerization and structural changes in the early intermediates, K and KL. Conformational changes of the retinal chromophore and rearrangements of the HBN in the retinal binding pocket revealed by the simulations and QM/MM optimizations are described below. The energetics of the K and KL formations are analyzed. The molecular mechanism of the absorption spectral shifts of the intermediates are also discussed.

Photoisomerization

Using different initial configurations (coordinates and velocities) selected from the ground state equilibrium trajectory at time intervals of 5 ps, 40 isomerization MD trajectories, 20-ps-long each, were calculated. After the photoexcitation, the trajectories stayed around the Franck-Condon region transiently before proceeding to the 13-*cis* configuration. The average lifetime of the excited state was 116 fs. Because in the present model, the vibrational relaxation of the in-plane skeleton modes of the polyene part contributions to the transition from the Franck-Condon region (H) to a fluorescent state (I) is not described, the lifetime of the excited state is expected to be shorter than the experimental one (the formation time of the vibrationally hot photoproduct, J, is ~500 fs). The lifetime is rather sensitive to the potential profile describing torsion around the C_{13}═C_{14} bond, and precise molecular models are therefore needed to reproduce the experimentally observed lifetime.

The simulations provided an insight into the directionality of the isomerization, i.e., clockwise or counter clockwise around the C_{13}═C_{14} bond. The two possible directions of the isomerization result in the rotation of the N—H bond of the Schiff base toward Asp-85 or toward Asp-212 (Fig. 4), respectively. In our simulations, all isomerizations happened toward Asp-212. The unidirectional isomerizations

toward Asp-212 have been also reported in a recent computational study by Warshel and Chu (2001).

Because a symmetric function has been used for the description of the C_{13}═C_{14} dihedral potential (Fig. 4), the unidirectionality of the isomerization is purely due to forces of the environment. Our previous MD and QM/MM studies showed that the conformation of the $C_{13} \sim N_{\zeta}$ part of the chromophore in the BR ground state is twisted and the N—H bond of the Schiff base is tilted toward Asp-212 (Tajkhorshid et al., 2000; Hayashi and Ohmine, 2000). Particularly, the C_{12}—C_{13}═C_{14}—C_{15} dihedral angle deviates considerably (19° in the QM/MM optimized geometry) from planarity. A twisted conformation of retinal toward Asp-212 in BR, which was also observed in the present study, originates from the forces of the environment that favor the isomerization in the direction of Asp-212.

The unidirectional torsion arises from two kinds of interactions of retinal with the surroundings. One is the steric interactions with residues constituting the retinal binding pocket. Because the binding pocket exhibits a slightly bent shape, the conjugated chain of retinal adjusts itself to the binding pocket by twisting around the C_{13}═C_{14} and C_{15}═N_{ζ} double bonds (Tajkhorshid et al., 2000; Hayashi and Ohmine, 2000). Previous MD simulations (Tajkhorshid et al., 2000) have clearly shown that reduction of the bend of the binding pocket by replacing Trp-86 by Ala results in the relaxation of torsion at those double bonds. The other interaction is due to the strong hydrogen bond of the Schiff base N—H bond with Wat-402. The resulting twisted structure of the chromophore could not be observed when Wat-402 was described by the TIP3P model, instead of the present water model that includes three body effects and explicit interaction of lone pairs. Therefore, strong hydrogen-bonds between the Schiff base, Wat-402, and Asp-85 are essential for the twisted retinal conformation that ensures a unidirectional photoisomerization.

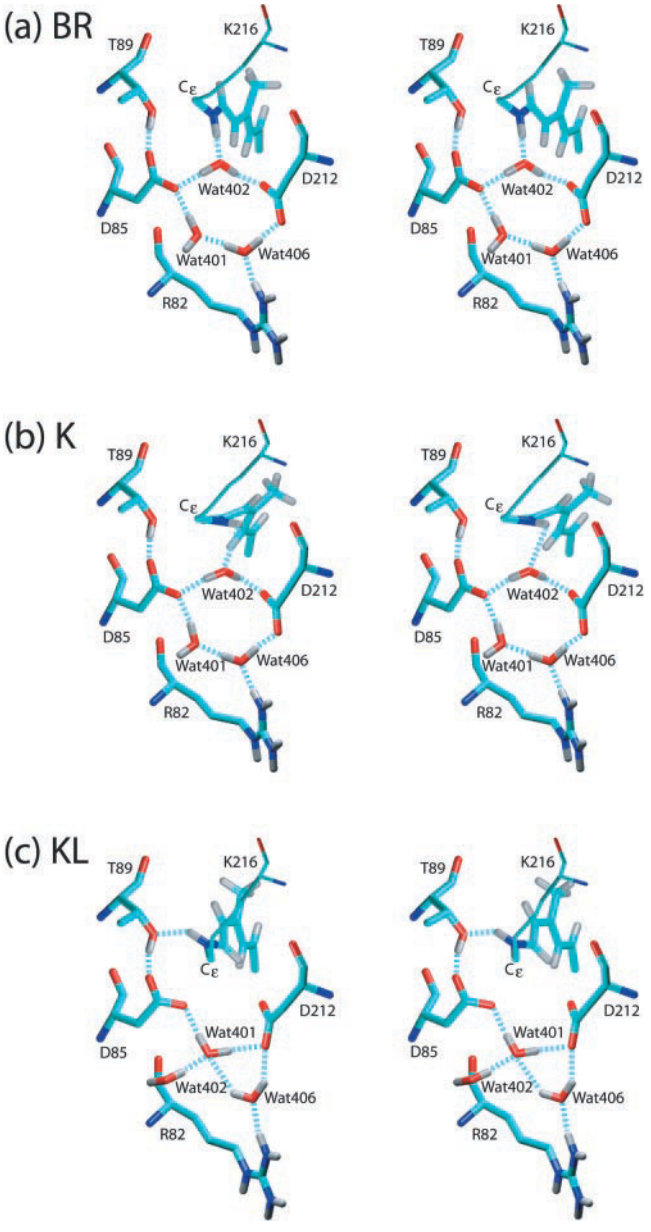

FIGURE 6 Structural changes in the vicinity of the Schiff base in the early phase of the photocycle, modeled in the present study. Stereo views are shown for the QM/MM optimized structures of (*a*) BR, (*b*) K, and (*c*) KL. The hydrogen-bonds are depicted as dashed lines. Wat-402 in the calculated KL structure corresponds closely to Wat-401 in the x-ray structure model of K (Edman et al., 1999), and Wat-401 in the present model is suggested to be the missing water in the x-ray model (see the KL intermediate section).

The K intermediate

To proceed to the first intermediate, eight isomerization trajectories were continued for 200 ps. All runs resulted in almost the same 13-*cis* photoproduct, in which the chromophore had a strongly deformed structure. Fig. 6 *b* displays the QM/MM energy minimized structure of this photoproduct, assigned to the K (or K_{LT}) intermediate. One can clearly see that the chromophore is largely twisted in the $C_{13} \sim N_{\zeta}$ region, and the N—H bond of the Schiff base is almost perpendicular to the membrane normal and pointing toward Asp-212. In a fully planar 13-*cis* conformation of the chromophore, the N—H bond is expected to point "up" (parallel to the membrane normal). However, in none of the eight simulations performed at room temperature was a completely relaxed planar 13-*cis* conformation observed. The N—H bond maintains its interaction with Wat-402 and Asp-212 in the K intermediate, thus preventing the chromophore from relaxing into a planar conformation.

Table 3 compares geometrical parameters of the chromophore in the QM/MM optimized structures of BR and K. In K, the strong torsions are mainly localized in the $C_{13} \sim N_{\zeta}$ region. Especially, the C_{14}—C_{15}═N_{ζ}—C_{ε} and C_{12}—C_{13}═C_{14}—C_{15} double bonds are largely twisted by

TABLE 3 Geometrical features of the chromophore in the BR, K, and KL states

	BR	K	KL
C_{15}═N_{ζ}—C_{ε}—C_{δ}	−112.8	−149.3	120.6
C_{14}—C_{15}═N_{ζ}—C_{ε}	−166.8	149.2	−157.2
C_{13}═C_{14}—C_{15}═N_{ζ}	−178.2	162.2	−171.4
C_{12}—C_{13}═C_{14}—C_{15}	−161.3	−25.4	26.4
C_{11}═C_{12}—C_{13}═C_{14}	173.7	−176.1	170.6
C_{10}—C_{11}═C_{12}—C_{13}	−172.7	168.3	−168.0
C_9═C_{10}—C_{11}═C_{12}	−175.0	−172.6	−179.5
C_8—C_9═C_{10}—C_{11}	−178.0	−171.3	−176.0
C_7═C_8—C_9═C_{10}	−172.6	−172.9	−176.1
C_6—C_7═C_8—C_9	176.9	174.6	177.8
C_5═C_6—C_7═C_8	169.7	168.0	177.1
ϕ_{NH}*	19.8	82.3	236.1
ϕ_{C20}†	158.9	128.7	155.3

*Angle of the N—H bond of the Schiff base to the membrane normal.
†Angle of the C_{13}—C_{20} bond to the membrane normal.
Angles are in degree.

30° and 25°, respectively. Although dihedral angles of the other half of the polyene chain, C_{13} to C_5, do not significantly deviate from 180°, small rotations around C_9═C_{10} and C_{11}═C_{12} result in an overall twist in this half. Consequently, the C_{20} methyl group attached to C_{13} is tilted toward Asp-212, and the angle of the C_{13}—C_{20} bond to the membrane normal in K differs by 30° from that in the BR ground state (for the numbering of retinal carbons, see Fig. 1).

Fig. 7 *a* schematically depicts the HBN in the K intermediate. The HBN does not undergo large conformational changes upon the formation of K, as can be discerned by comparison of Figs. 3 (BR) and 7 (K). Only minor changes in the hydrogen-bond distances were found, except for the hydrogen bonds between H_{ζ} of the Schiff base and Wat-402. The isomerization of the chromophore moves the H_{ζ} atom upward, resulting in a weakened hydrogen bond between the Schiff base and Wat-402. The distance between Wat-402:H_2 and Asp-85:$O_{\delta 1}$ also slightly increases due to the reduction of charge transfer and polarization effects from the Schiff base.

The strongly twisted chromophore in our K intermediate presents a remarkable difference from the x-ray crystallographic model of Edman et al. (1999), in which the chromophore conformation is assumed planar. Furthermore, the K intermediate in the present study involves only minor changes of the HBN, as seen in Fig. 6, whereas in the x-ray model (Fig. 2 *b*) significant changes of the HBN are observed as discussed in the Introduction section. In the present K model, Wat-402 occupies almost the same position as in BR, and the hydrogen-bond between Thr-89 and Asp-85 is not broken.

The present K model is, however, in keeping with the results of LT-RR (Pande et al., 1981; Braiman and Mathies, 1982) and LT-FTIR (Bagley et al., 1982; Rothschild and Marrero, 1982) spectroscopic measurements, which indicate a strong enhancement of the hydrogen-out-of-plane (HOOP) vibrational peaks of the chromophore upon the formation of K. One of the prominent peaks at ~960 cm^{-1} has been assigned to the 15-HOOP mode (Braiman and Mathies, 1982). The intensities of the HOOP modes are small in the planar conformation and become large when the structure is distorted. Hence the torsional deformation around the Schiff base in our K model is consistent with the large HOOP peaks in the LT-RR and LT-FTIR spectra.

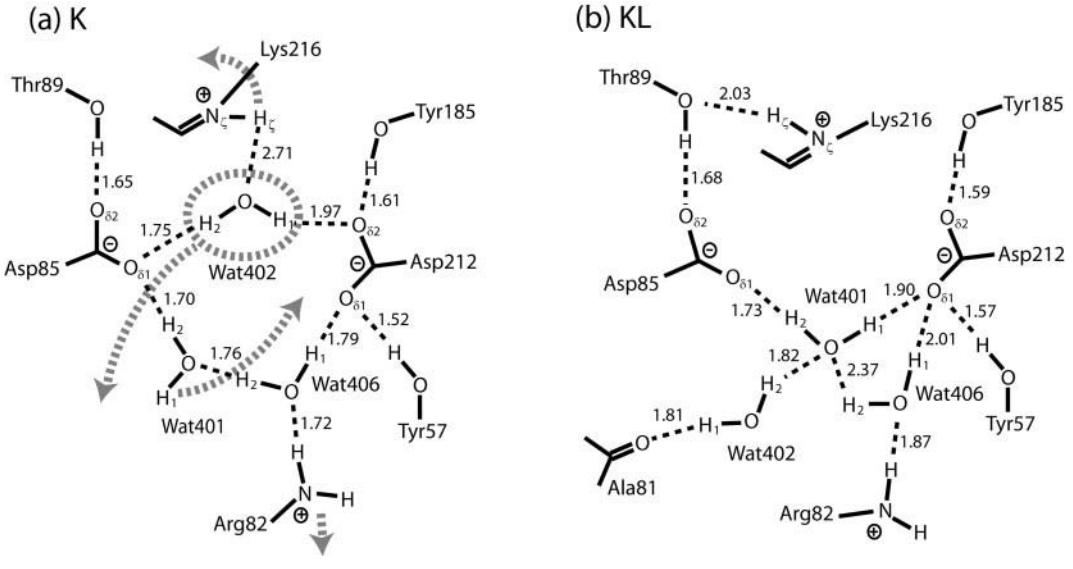

FIGURE 7 Schematic representations of the HBN in the binding pocket in (*a*) K and (*b*) KL. Dashed thin lines represent hydrogen-bonds. Distances of the hydrogen-bonds are shown in Å. Dashed thick arrows in gray illustrate conformational changes of the hydrogen-bond network during the K-to-KL transition.

The IR spectral shape of the HOOP peak at 960 cm^{-1} is altered by the mutation of Thr-89 to Cys (Kandori et al., 1999). The present model of K can explain this mutation effect. The H_{15} atom is close to Thr-89:O_γ (2.58 Å), and replacement of the O atom by the S atom, which is larger, in the T89C mutant can affect the spectral shape of the 15-HOOP. Contrary to the x-ray model (Edman et al., 1999), FTIR measurements (Kandori et al., 1998b, 1999, 2001) indicate that the hydrogen-bond between Thr-89 and Asp-85 becomes stronger upon the formation of K. The distance between Thr-89:H_γ and Asp-85:O_δ in the simulated K intermediate is 0.01 Å shorter than that in BR (Figs. 3 and 7 *a*), implying a stronger hydrogen-bond, and thus supporting the FTIR result. The almost perpendicular orientation of the N—H bond of the Schiff base to the membrane normal is also in good agreement with a recent polarized FTIR measurement (Kandori et al., 2002).

The KL intermediate

As discussed above, the chromophore has a strongly twisted conformation in K because the Schiff base maintains its connection to Wat-402. Nevertheless, the hydrogen-bond is rather weak in K and the distance between H_ζ of the Schiff base and Wat-402:O (2.7 Å) is remarkably larger compared to other hydrogen bonds (1.5 ~ 1.8 Å), as seen Fig. 7 *a*. Furthermore, during the simulations, the distance between the Schiff base and Wat-402 frequently becomes longer due to thermal fluctuation and tension by the strongly deformed chromophore in the Schiff base region. Breaking of the hydrogen-bond between the Schiff base and Wat-402 seems to be a prerequisite for the relaxation of the chromophore to a planar conformation in which the N—H bond points "up," i.e., toward the cytoplasmic side. Although none of the isomerization trajectories applying the set 1 force field used in the modeling of the K intermediate resulted in the complete cleavage of this hydrogen-bond, it is likely that the dissociation of the hydrogen bond leads to a transition from K to the next intermediate, KL.

Because the lifetime of K can be as long as 100 ns according to a recent TR-FTIR study (Doiumaev and Braiman, 1997), it is not feasible to observe the decay of K in MD simulations. Furthermore, the lifetime of K can increase even further due to the strengthened hydrogen bond between the Schiff base and Wat-402 in the set 1 force field. Unfortunately, it is rather difficult to determine empirical potential functions that can quantitatively describe the dissociation of hydrogen bonds that involve strong electronic interactions. To accelerate the decay of the K intermediate, therefore, we used the set 2 force field, which does not include the additional function for the hydrogen bond (see MD simulations section), and repeated the simulations to examine the dynamics of the photoproducts when this hydrogen bond can be easily broken.

Starting from the initial configurations taken from the BR equilibrium trajectory at time intervals of 10 ps, 32 isomerization trajectories, 80-ps-long each, were computed. The additional hydrogen-bond function in the set 1 force field was turned off at the beginning of isomerizations. The absence of the strong hydrogen bond did not affect the dynamics of the isomerization; all isomerizations took place toward Asp-212, as seen in the simulations of the K intermediate. In addition, the first photoproduct is also similar to the K intermediate obtained in the simulations with the set 1 force field, i.e., the chromophore is strongly deformed in the Schiff base region, and the N—H bond is perpendicular to the membrane normal.

After the formation of the K intermediate characterized as the first photoproduct, however, approximately two-thirds of the trajectories (21 in the 32 trajectories) proceeded to a second stable photoproduct in 80 ps. The remaining 11 trajectories stay in K on this time scale. Because the transition is a stochastic process, the 11 trajectories should reach the same second stable state after a longer time.

The excitation energy of the second photoproduct is red shifted from BR and blue shifted from K (see below). Therefore, we assign this state to the KL intermediate. Fig. 8 shows the QM/MM optimized structure of the KL intermediate. The K-to-KL transition is characterized by significant structural changes in the retinal binding pocket, as illustrated schematically in Fig. 7. The first event is a complete dissociation of the hydrogen bond between the Schiff base and Wat-402, which persists in the K intermediate. The dissociation leads to conformational relaxation of the chromophore to the 13-*cis* planar form, where the N—H bond of the Schiff base points to the cytoplasmic side and starts to establish a weak hydrogen-bond with Thr-89:O_γ. Along with formation of the hydrogen bond, the Schiff base part of the chromophore becomes twisted again but in the opposite direction to the K intermediate. One can discern this whiplash motion in Fig. 6 *c*, which displays the retinal binding site in KL, the hydrogen-bond between the Schiff base and Thr-89:O_γ and the twist in the Schiff base region. As will be discussed in the next section, the distorted conformation of the Schiff base is stabilized by electrostatic interaction with Asp-85, Asp-212, and Thr-89.

The geometrical features the chromophore in the KL intermediate are listed in Table 3. The C_{12}—C_{13}═C_{14}—C_{15} dihedral angle deviates by 26° from the planar conformation. Although the C_{14}—C_{15}═N_ζ—C_ε and C_{13}═C_{14}—C_{15}═N_ζ dihedral angles are also twisted considerably, the torsions are somewhat relaxed compared with that in the K intermediate. The relaxed torsions are consistent with the LT- and TR-FTIR and TR-RR measurements, where the 15-HOOP mode in KL (~980 cm^{-1}) exhibits a high frequency shift from that in the K intermediate (960 cm^{-1}) (Rothschild et al., 1985; Sasaki et al., 1993; Weidlich and Siebert, 1993; Hage et al., 1996; Dioumaev and Braiman, 1997; Althaus et al., 1995). As previously shown

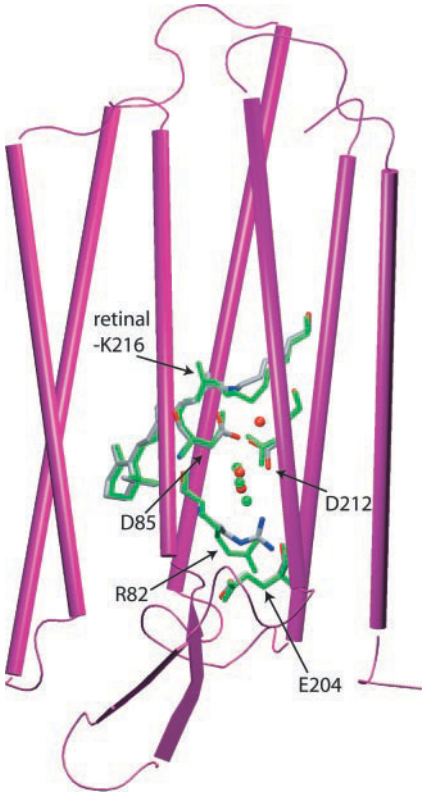

FIGURE 8 Structures of the K and KL intermediates. The seven transmembrane helices are shown as cylinders; loops are shown in tube representation; β-strands are drawn as ribbons. The retinal chromophore and key amino acids are highlighted (K is shown in *gray*, *blue*, and *red*; KL is shown in *green*). Water molecules (W-401, W-402, and W-406) are represented as red (K) and green (KL) spheres.

(Tajkhorshid et al., 1999; Tajkhorshid and Suhai, 1999), the H_{15} atom carries a large positive partial charge. The strong hydrogen bond between H_{15} and Asp-212:O_δ with 2.52 Å distance further stabilizes the twisted conformation in the Schiff base region. This hydrogen bond can, therefore, also contribute to the aforementioned high frequency shift of the 15-HOOP mode, because the interaction leads to a steeper potential well along a librational motion of the C_{15}—H_{15} bond that corresponds to the HOOP motion.

One also notices in Fig. 6 *c* and 8, *a* large movement of the Lys-216 chain during the K-to-KL transition. In particular, the N_ζ—C_ε single bond rotates by 90.2° (Table 3), and the C_ε atom moves down (Fig. 6 *c*). The conformational change of the chromophore-Lys-216 moiety causes a significant rearrangement of the HBN in the binding site. As clearly seen in Fig. 6 *c*, Wat-402 is dislocated from its position in the BR and K states (between the Schiff base, Asp-85, and Asp-212). Due to the complete dissociation of its hydrogen bond with the Schiff base, and steric interaction with the Lys-216:C_ε, Wat-402 is forced to move toward the extracellular side, initiating an overall rearrangement of the HBN. Wat-401 moves and bridges between Asp-85 and Asp-212, and, as a result, the carboxylate group of Asp-85 rotates slightly. The dislocation of Wat-402 also triggers a downward movement of Arg-82 (1.5-Å displacement at Arg-82:C_ζ) during the K-to-KL transition, as clearly seen in Fig. 8. A remarkable downward shift of the G helix, induced by the conformational change of Lys-216, is also observed in the KL structure.

Several structural features discussed above for the KL intermediate are actually consistent with the x-ray crystallography model of K (Edman et al., 1999). The dislocation of Wat-402 is in good agreement with the strong negative density in the K—BR difference electron density map. In addition, a significant movement of the Lys-216 side-chain around the C_ε atom and the downward shift of the G helix are common to both models. Furthermore, the carboxylate group of Asp-85 in our KL model is rotated as observed in the x-ray K model, although in our KL model this rotation is smaller and the hydrogen bond between Thr-89 and Asp-85 is not broken. Therefore, the x-ray model closely corresponds to the KL intermediate obtained in this study.

The x-ray measurements have been carried out for an intermediate state trapped at 110 K, a temperature 33 K higher than the liquid nitrogen temperature (77 K) used for trapping the K intermediate in spectroscopic studies. This slightly higher temperature might give rise to a mixture of the K and KL states. According to our model, the K formation involves only minor structural changes of the HBN. Therefore, it is likely that the observed difference electron density map is mainly due to structural differences between the BR and KL states. The present models show that the conformations of the chromophore around the Schiff base in K and KL are remarkably different (see Fig. 6, *b* and *c*, and Table 3). The inhomogeneity due to the presence of the two K-like species can also account for the absence of a positive density around the Schiff base region of the chromophore in the x-ray difference electron density map (Edman et al., 1999).

The present KL model also indicates the location of Wat-402, which has not been identified in the x-ray K model. According to our model, Wat-402 moves to a position that closely corresponds to the position of Wat-401 in the x-ray model of K. Therefore, the missing water in the x-ray model is the water bridging between Asp-85 and Asp-212 in our KL model (Wat-401 in Fig. 6 *c*). In fact, there seems to be a positive density at this position in the x-ray difference electron density map (see Fig. 5 in Pebay-Peyroula et al., 2000), although no water molecule is modeled at this position in the x-ray structure (PDB code, 1QKO).

The downward movement of Arg-82 toward the extracellular side in our KL model is not reported in the x-ray crystallographic study. This disagreement may be due to the different temperatures used for generating the intermediate state. In the x-ray study, the low temperature (110 K) was maintained throughout the experiments, whereas in the

TABLE 4 Changes of QM/MM energies ($E_{QM/MM}$*) upon the formation of K and KL, and their additive contributions,† E^0,‡ $V^{ES}_{QM—MM}$,§ $V^{LJ}_{QM—MM}$,¶ $V^{BAD}_{QM—MM}$,‖ and $E^{ERO}_{QM(MM)}$ in kcal/mol**

	$E_{QM/MM}$		E^0	$V^{ES}_{QM—MM}$	$V^{LJ}_{QM—MM}$	$V^{BAD}_{QM—MM}$	$E^{ERO}_{QM(MM)}$
K—BR	16.2††	23.1#	11.9	23.3	−8.5	−0.2	−3.4
KL—BR	29.0††	4.5#	7.1	6.7	−8.7	0.1	−0.5

*A sum of the energy of the QM region and the QM-MM interaction. The energies were evaluated for two QM/MM system, system A (the QM region consists of retinal-Lys-216, Asp-85, Asp-212, Wat-401, Wat-402, and Wat-406) and system B (the QM region consists of retinal-Lys-216).
†Additive energies were computed for system B.
‡QM energy in isolated condition.
§Electrostatic interaction between the QM and MM regions.
¶Lennard-Jones interaction between the QM and MM regions.
‖Bond, angle, and dihedral energies at the QM—MM boundary.
**Electronic reorganization energy.
††Results for system A.
#Results for system B.

present study the KL state was obtained by simulations at room temperature (300 K). Therefore, in the simulations we may observe structural fluctuations that cannot be detected in low temperature experiments. It is noted that the downward movement of Arg-82 has been observed in x-ray crystallographic structures of the later states, L (Royant et al., 2000) and M (Luecke et al., 1999b, 2000; Sass et al., 2000; Facciotti et al., 2001). The movement in the present KL model is, however, much smaller than the motions observed in the x-ray structures of L and M. This small movement is induced by the HBN rearrangement, especially the downward migration of Wat-402, upon the formation of KL.

Energetics of the early intermediates

As seen in the previous sections, the chromophore experiences significant conformational changes during the formation of the early intermediates, resulting in the HBN rearrangement in the retinal binding pocket. Understanding the energetics related to these conformational changes provides an insight into the molecular mechanism of the energy storage in the early phase of the pump cycle. We therefore decomposed and analyzed the QM/MM energies, $E_{QM/MM}$ (Eqs. 3 and 4), calculated for the early intermediate states. $E_{QM/MM}$ is defined as the sum of the energies of the QM region itself and its interaction with the MM region. Details of the method are described in the QM/MM energy decomposition analysis.

Table 4 lists the differences in $E_{QM/MM}$ between K, KL, and BR. The difference in $E_{QM/MM}$ between K and BR for system A is 16.2 kcal/mol. Because the MM region in system A stays almost unchanged upon the formation of K (see the K intermediate section), energy of the MM region, E_{MM}, in K is expected to be almost the same as in BR. Thus, an enthalpy change, i.e., energy change of the whole system, upon the formation of K can be well described by the energy difference in $E_{QM/MM}$ alone. The enthalpy change estimated in the present study is in good agreement with the experimental value of 16 kcal/mol (Birge and Cooper, 1983; Birge et al., 1989).

To calculate the contribution of the chromophore's conformational change alone, we also evaluated $E_{QM/MM}$ for system B, in which only the chromophore is included in the QM region, and Asp-85, Asp-212, and water molecules of the binding pocket reside in the MM region. The difference in $E_{QM/MM}$ between K and BR for system B is 23.1 kcal/mol, which is 6.9 kcal/mol larger than for system A. The difference is due to the slight changes in the structure and electronic interaction of nonretinal groups participating in HBN (Figs. 3 and 7).

Table 4 also summarizes the decomposed contributions to $E_{QM/MM}$ for system B (see QM/MM energy decomposition analysis section). The difference in E^0 is due to the conformational change of the chromophore. The strong torsion around the Schiff base region in K accounts for the large E^0 difference between K and BR (11.9 kcal/mol). Change of the chromophore-protein interactions also contributes to $E_{QM/MM}$. The electrostatic stabilization $V^{ES}_{QM—MM}$ in K is significantly smaller (23.3 kcal/mol) than in BR. Upon the formation of K, the H_ζ atom of the Schiff base moves away from such groups as Asp-85, Asp-212, and Wat-402, resulting in the weakening of the electrostatic stabilization. The changes of the electrostatic stabilization effects of Asp-85, Asp-212, and Wat-402 are estimated to be 4.4, 5.6, and 16.5 kcal/mol, respectively. On the other hand, the LJ interaction energy, $V^{LJ}_{QM—MM}$, significantly decreases (−8.5 kcal/mol) upon the formation of K. This drastic decrease is mainly due to the reduced strong short-range repulsion between the Schiff base and Wat-402 (−8.8 kcal/mol). The ERO energy, $E^{ERO}_{QM(MM)}$, also gives a stabilizing contribution (−3.4 kcal/mol), consistent with the large destabilizing contribution of $V^{ES}_{QM—MM}$ (Sec. 2.4).

Altogether, upon the formation of K, the energy (16.2 kcal/mol) is stored in the form of the conformational distortion of the chromophore (E^0 = 11.9 kcal/mol) and the weakening of the interaction of the Schiff base with the surrounding polar residues ($V^{ES}_{QM—MM}$ + $V^{LJ}_{QM—MM}$ +

$E^{ERO}_{QM(MM)}$ = 11.4 kcal/mol), part of which is compensated by the structural and electronic changes of the HBN in the binding pocket (−6.9 kcal/mol). This scheme is comparable with the results of Birge and Cooper (1983) suggesting that roughly one-half of the energy is stored in the form of the changes of the electrostatic interaction.

The analysis of energetics for KL is also summarized in Table 4. The difference in $E_{QM/MM}$ between KL and BR for system A is 29.0 kcal/mol, showing an energy increase by 12.8 kcal/mol from K to KL. This apparent endothermic change is due to the fact that the energy change of the MM region, which experiences conformational changes during the K-to-KL transition, is not included in our analysis; $E_{QM/MM}$ does not include some of the energy changes caused by the extensive rearrangement of the HBN, e.g., the movement of Arg-82 toward the extracellular side in the K-to-KL process (see the KL intermediate section). In fact, during the K-to-KL transition, the side chain of Arg-82 was found to gain large electrostatic stabilizations from Glu-194 (−10.9 kcal/mol) and Thr-205 (−3.4 kcal/mol) located at the extracellular end of the channel in the MM region, and those energies are not included in $E_{QM/MM}$. After taking into account such effects, it becomes evident that, despite the apparent increase of $E_{QM/MM}$ (12.8 kcal/mol), the energy of the KL intermediate is not higher than K.

The increase of $E_{QM/MM}$ from BR to KL in system B was estimated to be rather small (4.5 kcal/mol) compared with increase from BR to K (Table 4). The increasing stabilization of the chromophore during the K-to-KL transition implies that the energy, which was mainly stored in the chromophore itself and its interaction with the surroundings in K, is now partially used to rearrange the HBN in the extracellular channel, as seen in the KL intermediate section. The contribution of the conformational distortion of the chromophore, E^0, is still large (7.1 kcal/mol) in KL, but 4.8 kcal/mol smaller than K. This is consistent with the relaxed torsion of the Schiff base group in KL, as seen in Table 3. Compared with the K intermediate, the chromophore-protein electrostatic interaction (6.7 kcal/mol) is significantly smaller in KL. Although the hydrogen bond between the Schiff base and Wat-402 completely dissociates during the transition of BR to KL and the chromophore loses large electrostatic stabilization energy (20.8 kcal/mol), the loss is compensated by stabilization effects of Asp-85 (−10.0 kcal/mol), Thr-89 (−3.4 kcal/mol), and Asp-212 (−6.7 kcal/mol). Together with the change of the LJ interaction (−8.7 kcal/mol) and ERO (−0.5 kcal/mol) contributions, the interaction of the chromophore with its surroundings gives a stabilizing contribution of −2.6 kcal/mol.

It is noteworthy that the aforementioned stabilization of Arg-82 by Glu-194 and Thr-205 in the K-to-KL transition accompanies a similar amount of destabilization due to its separation from Asp-212 (11.0 kcal/mol) and Asp-85 (3.4 kcal/mol), which are main reasons for the observed increase in $E_{QM/MM}$ of system A. Evidently, Arg-82 maintains a delicate balance of its interaction with those residues during its movement. Such a balance may account for the conformational flexibility of Arg-82.

TABLE 5 Excitation energies (E_{ex}) of the retinal chromophore in the BR, K, and KL states, and contributions to the excitation energy, excitation energy of the isolated chromophore (E^0_{ex}), electrostatic interaction between chromophore and protein matrix ($\Delta V^{ES}_{ch—pr}$), and electronic reorganization energy of the chromophore ($\Delta E^{ERO}_{ch(pr)}$) (all energies are in kcal/mol)

	E_{ex}	E^0_{ex}	$\Delta V^{ES}_{ch—pr}$	$\Delta E^{ERO}_{ch(pr)}$
BR	98.3 (50.3†)	68.3	23.3	6.7
K*	−10.1 (−3.5‡)	−4.1	−2.2	−3.8
KL*	−3.5 (−1.8†)	−3.2	1.4	−1.6

*Values are relative to BR.
†Absorption maxima at room temperature (Lozier et al., 1975).
‡Absorption maxima at 77 K (Birge et al., 1989).

Excitation energies

bR possesses photochromic properties and changes its absorption spectrum during the photocycle (Lozier et al., 1975). In the K and KL intermediates, the absorption maxima exhibit red shifts from the absorption maximum in the BR state. To assess the simulated models of the early intermediates, we computed excitation energies of the chromophore by means of the CASSCF QM/MM method (see QM/MM excitation energy calculations section). Table 5 lists the excitation energies for the BR, K, and KL states. The absolute values are largely overestimated compared with the experimental ones, mainly due to the lack of the σ-π dynamic electronic correlation in the CASSCF description of the ionic S_1 state. Nevertheless, the calculations show red shifts in the maximal absorption of the chromophore upon the formations of the K and KL states, in agreement with the experimental findings (Lozier et al., 1975; Shichida et al., 1983), although the calculated spectral shifts are too large compared with experimental values.

We have also further analyzed the excitation energies to determine the mechanism of the spectral shifts and to estimate possible sources of the error in the calculated spectral shifts. The excitation energies, E_{ex}, were decomposed into three contributions, E^0_{ex}, $\Delta V^{ES}_{ch—pr}$, and $\Delta E^{ERO}_{ch(pr)}$, as described in QM/MM excitation energy calculations section. These contributions are listed in Table 5 for the BR, K, and KL states.

In the K intermediate, E^0_{ex} contributes −4.1 kcal/mol to the red-shift relative to BR. This is due to the strongly deformed conformation of the chromophore in the Schiff base region. In particular, strong twists of the C_{15}═N_ζ and C_{13}═C_{14} double bonds destabilize the highest occupied π orbital and stabilize the lowest unoccupied π^* orbital, leading to a smaller excitation energy. The contribution of E^0_{ex} to the red shift may be overestimated here, mainly due to a

poor description of correlations between the σ and π electrons. The other large contributions come from $\Delta V^{ES}_{ch—pr}$ (-2.2 kcal/mol) and $\Delta E^{ERO}_{ch(pr)}$ (-3.8 kcal/mol). They originate from a large reduction of the electrostatic interaction of the S_0 state with the protein environment during the BR-to-K transition, as discussed in Energetics of the early intermediates section (Table 4). The weaker stabilization of the positive charge results in the red-shift contribution of $\Delta V^{ES}_{ch—pr}$ (QM/MM excitation energy calculations section). At the same time, a weaker interaction gives rise to less polarization of the chromophore in the S_1 state, leading to the red-shift contribution of $\Delta E^{ERO}_{ch(pr)}$.

The red-shift contributions of $\Delta V^{ES}_{ch—pr}$ and $\Delta E^{ERO}_{ch(pr)}$ might be also overestimated in our calculations. The HF method used for the geometry optimization of the chromophore is known to overestimate bonding characters, and, therefore, the torsions in the Schiff base region observed in K are expected to be underestimated. Consequently, the N—H bond tends to point away from the extracellular side too much, resulting in a too weak electrostatic interaction between the Schiff base and Wat-402. Our preliminary calculations showed that the distance between H_ζ of the Schiff base and Wat-402:O can be shorter at only a small energy cost, e.g., 0.7 Å shorter at 3 kcal/mol energy increase, whereas the excitation energy is rather sensitive to this distance.

In the KL intermediate, there also exists a red-shift contribution of E^0_{ex}, as seen in Table 5, due to the chromophore torsion in the Schiff base region (see Fig. 6 *c* and Table 3). On the other hand, the shifts of $\Delta V^{ES}_{ch—pr}$ and $\Delta E^{ERO}_{ch(pr)}$ are somewhat complicated; $\Delta V^{ES}_{ch—pr}$ gives a blue-shift contribution (1.4 kcal/mol), whereas the electrostatic stabilization energy of the S_0 state with the surroundings in KL is slightly reduced (6.7 kcal/mol, see Table 4) from that in BR. This stems from a weaker electrostatic stabilization in S_1 due to a less polarized electronic wave function. One can see that the counterpart of the $\Delta V^{ES}_{ch—pr}$ contribution arises in $\Delta E^{ERO}_{ch(pr)}$; because of the weaker polarization, destabilization of the S_1 state by the electronic reorganization is also smaller. Hence $\Delta E^{ERO}_{ch(pr)}$ provides a red-shift contribution.

The KL intermediate was first introduced by Shichida et al. (1983) based on visible absorption experiments revealing an intermediate that was ~15 nm blue shifted from K. However, this absorption spectral shift has been questioned by another visible absorption experiment (Yamamoto et al., 1994) where no spectral shift was observed on a nanosecond time scale. The present results support a blue shift of the spectra in the K-to-KL transition. However, further calculations taking into account electronic correlation (Hayashi and Ohmine, 2000), polarization of the protein matrix (Houjou et al., 2001), and charge-transfer effects will be needed for a definitive understanding of the spectral shift.

DISCUSSION

In the present study, we propose structural models for two early intermediate states, K and KL, in bR's photocycle. The structures of the retinal chromophore and the HBN in the retinal binding site are remarkably different in K and KL. In K, the chromophore is strongly twisted in the Schiff base region, and the N—H bond points toward Asp-212. The strong torsion in the Schiff base is consistent with LT-FTIR and resonance Raman results, revealing a high intensity peak for the 15-HOOP mode (Pande et al., 1981; Braiman and Mathies, 1982; Bagley et al., 1982; Rothschild and Marrero, 1982). In KL, the chromophore is still twisted, but the N—H bond points toward Asp-85 and is hydrogen bonded to Thr-89. The structural changes in the Schiff base region during the K-to-KL transition are in keeping with the characteristic IR spectral change of the 15-HOOP mode observed by LT- and TR-FTIR and TR-RR spectroscopic studies (Rothschild et al., 1985; Sasaki et al., 1993; Weidlich and Siebert, 1993; Hage et al., 1996; Dioumaev and Braiman, 1997; Altaus et al., 1995).

A picosecond TR-RR spectroscopic study (Doig et al., 1991) has reported a large HOOP band in J, the intensity of which decreases significantly after 3 ps, and increases again in 10 to 40 ps. The authors have labeled the HOOP-silent state as K, and the following intermediate as KL, and concluded that the chromophore in the very early intermediate J is highly twisted, but it conformationally relaxes to a more planar form in K, and again undergoes torsions in KL. Because the time scale of the K-to-KL transition in the TR-RR measurement (10 to 40 ps) is completely different from that in the TR-FTIR one (~100 ns), K in TR-RR is considered to be a new state (K_p), different from K in TR-FTIR, and KL in TR-RR corresponds to K in TR-FTIR (Dioumaev and Braiman, 1997).

In the present study, no planar conformation of the chromophore corresponding to the K_p state was observed. However, it is possible that even a strongly twisted chromophore exhibits a weak Raman intensity of a HOOP mode in K_p due to thermal fluctuation. After the isomerization, the chromophore stores a large amount of excess energy that leads to vibrational excitations. In the short time of J formation, only torsional modes of the polyene skeleton that are directly coupled to the isomerization are vibrationally excited. Then, the excess vibrational energy in the torsional modes is transfered to the HOOP modes by intramolecular vibrational energy redistribution during the K_p formation. The highly excited vibrations of the HOOP modes can give rise to inhomogeneous broadenings of signals, possibly appearing as low intensity peaks. The intensities can recover through the vibrational cooling during the K_p-to-K transition.

The topology of the HBN in the vicinity of the Schiff base in K remains the same as in BR. Contrary to the x-ray crystallographic K model (Edman et al., 1999), no disloca-

tion of Wat-402 from the position between the Schiff base, Asp-85, and Asp-212 was observed in our K model. In the K-to-KL transition, on the other hand, remarkable hydrogen-bond rearrangements take place. Wat-402 is dislocated due to the complete dissociation of its hydrogen bond with the Schiff base and its steric interaction with Lys-216:C_ε. The resulting KL structure corresponds closely to the K intermediate found in the x-ray study (Edman, et al., 1999).

LT-FTIR experiments of Kandori et al. (1998b, 1999, 2001) have revealed that the hydrogen bond between Thr-89 and Asp-85 is stronger in K than in BR, in contradiction to the K model by the x-ray crystallography (Edman et al., 1999), where the carboxylate group of Asp-85 largely rotates and the hydrogen bond is completely broken. The present K and KL models can reconcile the apparent discrepancy; the low temperature vibrational spectroscopies observe K, whereas the x-ray crystallographic experiment actually observes KL.

A central question is how the early intermediates use the photon energy, initially stored through the electronic excitation of the chromophore, to enable bR to pump a proton during the relaxation processes. The present K model clearly indicates that the energy is stored in the form of chromophore's conformational deformation and weakened interactions between the Schiff base and the surrounding polar side chains and water molecules. In the K-to-KL transition, the chromophore partially relaxes its conformation and establishes stronger electrostatic interactions with the surroundings. However, the conformational relaxation of the chromophore also triggers the rearrangement of the HBN in the binding pocket. Wat-402 is pushed out to a less polar region and loses strong hydrogen-bonds to the negatively charged Asp-85 and Asp-212. The energy gain of the conformational relaxation of the chromophore is, therefore, used to produce a less stable hydrogen-bond configuration. It is noteworthy that the loss of a hydrogen bond between water and Asp-85 can drastically affect the energy profile of the proton transfer between the Schiff base and Asp-85, as shown previously by QM/MM calculations (Hayashi and Ohmine, 2000). Hence the rearrangement of the HBN in retinal's binding site is a key step in the primary proton transfer process of bR.

Because the HBN spans all regions of the extracellular half of the channel, the unstable water configuration in the binding pocket is expected to lead to overall conformational changes in this half (Edman et al., 1999). In fact, a downward displacement of Arg-82, a participant of the HBN, was observed in the present KL model. The downward displacement of Arg-82 is suggested to increase the pK_α of Asp-85 and decrease that of Glu-204, which is located at the extracellular end of the channel and is responsible for the proton release to the extracellular bulk water (Fig. 8). The unstable water configuration allows Arg-82 to be more flexible and accomplish the long range correlation between the primary proton transfer in the middle of the channel and the proton release to bulk water at the extracellular surface in the later L-to-M step.

In the KL state, the N—H bond of the Schiff base still points away from Asp-85, which is the acceptor in the primary proton transfer. After the KL state, therefore, further conformational changes of the chromophore are required to establish the proton pathway between the Schiff base and Asp-85 (Zhou et al., 1993). NMR studies (Hu et al., 2001; Herzfeld and Tounge, 2000; Hatcher et al., 2002) have suggested significantly twisted double bonds of the chromophore in the L and early M intermediates. Accordingly, the strong torsions around the double bonds appearing in the KL state are expected to persist or develop further in the KL-to-L step.

CONCLUSION

The availability of the high resolution x-ray structures of bR together with the accumulated spectroscopic information has set the stage for us to determine the atomic structural models of the early intermediates of bR's photocycle. We have performed MD simulations and QM/MM calculations to model the K and KL intermediates. The MD simulations were carried out with a faithful description of water molecules that takes into account electronic multibody effects. The intermediate structures obtained by the MD simulations of photoisomerization were refined by ab initio QM/MM geometry optimizations, which provide an accurate description of the electronic effects for the chromophore and the HBN. The excitation energies were also computed to identify the intermediates and to analyze the mechanism underlying their bathochromic shifts.

The present study proposes for the first time structural models for both K and KL intermediates. The models reveal important structural details, such as the chromophore conformation and the position of internal water molecules, which are not clearly observed in the x-ray crystallographic model of K. The simulated intermediates can also explain the prominent spectra of K and KL observed in FTIR and resonance Raman spectra and resolve the apparent disagreement between the x-ray structural and FTIR spectroscopic studies. Our QM/MM vibrational normal mode analyses also assign successfully the FTIR spectra of the HBN (Hayashi, Tajkhorshid, and Schulten, in preparation), and explains the underlying mechanism of the remarkable features of the FTIR spectra.

The present structures shed light on the mechanism of energy storage in the early stages of the bR's photocycle. In K, the strongly deformed chromophore and the weakened interaction of the Schiff base with the counter-ion groups and water are the means of storing the absorbed energy. During the K-to-KL transition, conformational relaxation of the chromophore induces significant HBN rearrangements that facilitate the proton transfers in later steps.

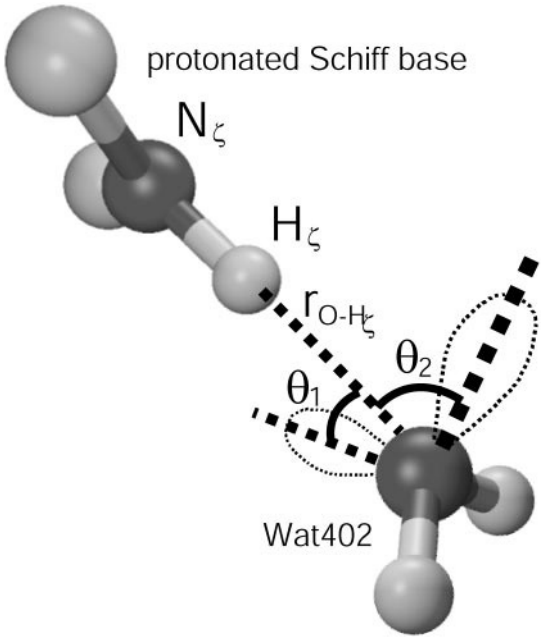

FIGURE 9 Schematic representation of geometrical parameters used in the augmenting potential describing the hydrogen bond interactions between Wat-402 and its neighbors.

In future studies, similar approaches combining MD and QM/MM simulations can be used to elucidate other molecular processes in the photocycle of bR, especially the primary proton transfer in the L-to-M step, where the quantum mechanical treatments are necessary. Also, the applied QM/MM methodology together with an improved description of the HBN permits us to seek a more complete understanding of the ultra-fast excited state dynamics of photoisomerization of the chromophore inside the protein matrix.

APPENDIX

In the set 1 force field, the potential functions of hydrogen-bond interactions of Wat-402 with the Schiff base, Asp-85, and Asp-212 were augmented by an additional term,

$$E_{\text{add}} = E_{\text{NH—LP}} + E_{\text{O}_\delta\text{—}H}. \quad (6)$$

$E_{\text{NH—LP}}$ is the interaction energy between N—H of the Schiff base and lone pairs of Wat-402, described as

$$E_{\text{NH—LP}}(r_{\text{O—H}_\zeta}, \theta_1, \theta_2) = \sum_{i=1,2} E_{\text{tap}}(\theta_i) A_{\text{NH—LP}} \times e^{-\alpha_{\text{O—H}_\zeta}^{-2}(r_{\text{O—H}_\zeta} - r_{\text{O—H}_\zeta}^0)^2} e^{-\alpha_\theta^{-2}\theta_i^2}. \quad (7)$$

The variables, $r_{\text{O—H}_\zeta}$ and θ_i, are schematically shown in Fig. 9. $r_{\text{O—H}_\zeta}$ is the distance between the O atom of Wat-402 and the H_ζ atom of the Schiff base. θ_i is the angle between the lone pair orbital and $r_{\text{O—H}_\zeta}$. Directions of the lone pairs are set to be tetrahedral, i.e., the angle between the lone pairs is 109.5°. $E_{\text{tap}}(\theta_i)$ is a tapering function applied to remove the disconnectivity around $\theta_i = 180°$. $E_{\text{O}_\delta\text{—H}}$ describes the short-range interactions between the H atoms of Wat-402 and O_δ of Asp-85 and Asp-212, as

$$E_{\text{O}_\delta\text{—}H}(r_{\text{O}_\delta\text{—}H,1}, r_{\text{O}_\delta\text{—}H,2}) = \sum_{i=1,2} \left[A_{\text{O}_\delta\text{—}H} \left(\frac{r_{\text{O}_\delta\text{—}H}^0}{r_{\text{O}_\delta\text{—}H,i}} \right)^{10} + H(-r_{\text{O}_\delta\text{—}H,i} + r_{\text{O}_\delta\text{—}H}^0) B_{\text{O}_\delta\text{—}H}(r_{\text{O}_\delta\text{—}H,i} - r_{\text{O}_\delta\text{—}H}^0)^2 \right]. \quad (8)$$

$r_{\text{O}_\delta\text{—H},1}$ and $r_{\text{O}_\delta\text{—H},2}$ are distances between H_2 of Wat-402 and $O_{\delta 1}$ of Asp-85 and between H_1 of Wat-402 and $O_{\delta 2}$ of Asp-212, respectively. $H(r)$ is the Heavyside function.

The parameters were determined so as to reproduce the QM/MM interaction energies, as described in MD simulations section, $r_{\text{O—H}_\zeta}^0 = 1.58$ Å, $A_{\text{NH—LP}} = -10.7$ kcal/mol, $\alpha_{\text{O—H}_\zeta} = 1.14$ Å, $\alpha_\theta = 60.9°$, $r_{\text{O}_\delta\text{—H}}^0 = 1.62$ Å, $A_{\text{O}_\delta\text{—H}} = -3.5$ kcal/mol, and $B_{\text{O}_\delta\text{—H}} = 2000$ kcal/mol · Å^{-2}.

The authors are grateful to Prof. Kandori for stimulating discussions. The work is supported by the Roy J. Carver Charitable Trust, the National Institutes of Health (PHS5 P41RR05969-04), the National Science Foundation (MCB-9982629), and the Human Frontier Science Program Organization. The authors also acknowledge computer time provided by the Grant NRAC:MCA93S028. The molecular images in this paper were created with the molecular graphics program VMD (Humphrey et al., 1996) and rendered with Raster3D (Merritt and Bacon, 1997).

REFERENCES

Althaus, T., W. Eisfeld, R. Lohrmann, and M. Stockburger. 1995. Application of Raman spectroscopy to retinal proteins. *Isr. J. Chem.* 35: 227–251.

Bagley, K., G. Dollinger, L. Eisenstein, A. K. Singh, and L. Zimányi. 1982. Fourier transform infrared difference spectroscopy of bacteriorhodopsin and its photoproducts. *Proc. Natl. Acad. Sci. U.S.A.* 79:4972–4976.

Baudry, J., E. Tajkhorshid, F. Molnar, J. Phillips, and K. Schulten. 2001. Molecular dynamics study of bacteriorhodopsin and the purple membrane. *J. Phys. Chem. B.* 105:905–918.

Bayly, C. I., P. Cieplak, W. D. Cornell, and P. A. Kollman. 1993. A well-behaved electrostatic potential based method using charge restraints for deriving atomic charges: the RESP model. *J. Phys. Chem.* 97:10269–10280.

Belrhali, H., P. Nollert, A. Royant, C. Menzel, J. Rosenbusch, E. M. Landau, and E. Pebay-Peyroula. 1999. Protein, lipid and water organization in bacteriorhodopsin crystals: a molecular view of the purple membrane at 1.9 angstrom resolution. *Structure.* 7:909–917.

Ben-nun, M., F. Molnar, H. Lu, J. C. Phillips, T. J. Martínez, and K. Schulten. 1998. Quantum dynamics of retinal's femtosecond photoisomerization in bacteriorhodopsin. *Faraday Discuss.* 110:447–462.

Berendsen, H. J. C., J. P. M. Postma, W. F. van Gunsteren, A. Di Nola, and J. R. Haak. 1984. Molecular dynamics with coupling to an external bath. *J. Chem. Phys.* 81:3684–3690.

Birge, R. R., and T. M. Cooper. 1983. Energy storage in the primary step of the photocycle of bacteriorhodopsin. *Biophys. J.* 42:61–69.

Birge, R. R., T. M. Cooper, A. F. Lawrence, M. B. Masthay, C. Vasilakis, C.-F. Zhang, and R. Zidovetzki. 1989. A spectroscopic, photocalorimetric, and theoretical investigation of the quantum efficiency of the primary event in bacteriorhodopsin. *J. Am. Chem. Soc.* 111:4063–4074.

Braiman, M., and R. Mathies. 1982. Resonance Raman spectra of bacteriorhodopsin's primary photoproduct: evidence for a distorted 13-cis retinal chromophore. *Proc. Natl. Acad. Sci. U.S.A.* 79:403–407.

Braiman, M. S., T. Mogi, T. Marti, L. J. Stern, H. G. Khorana, and K. J. Rothschild. 1988. Vibrational spectroscopy of bacteriorhodopsin mu-

tants—light-driven proton transport involves protonation changes of aspartic-acid residue-85, residue-96, and residue-212. *Biochemistry.* 27: 8516–8520.

Brown, L. S., J. Sasaki, H. Kandori, A. Maeda, R. Needleman, and J. K. Lanyi. 1995. Glutamic acid 204 is the terminal proton release group at the extracellular surface of bacteriorhodopsin. *J. Biol. Chem.* 270: 27122–27126.

Bullough, P. A., and R. Henderson. 1999. The projection structure of the low temperature K intermediate of the bacteriorhodopsin photocycle determined by electron diffraction. *J. Mol. Biol.* 286:1663–1671.

Chon, Y.-S., J. Sasaki, H. Kandori, L. S. Brown, J. K. Lanyi, R. Needleman, and A. Maeda. 1996. Hydration of counterion of the Schiff base in the chloride-transporting mutant of bacteriorhodopsin: FTIR and FT-Raman studies on the effects of anion binding when Asp85 is replaced with a neutral residue. *Biochemistry.* 35:14244–14250.

Cornell, W. D., P. Cieplak, C. I. Bayly, I. R. Gould, K. M. Merz, Jr., D. M. Ferguson, D. C. Spellmeyer, T. Fox, J. W. Caldwell, and P. A. Kollman. 1995. A second generation force field for the simulation of protein, nucleic acids, and organic molecules. *J. Am. Chem. Soc.* 117: 5179–5197.

de Groot, H. J. M., G. S. Harbison, J. Herzfeld, and R. G. Griffin. 1989. Nuclear magnetic resonance study of the Schiff base in bacteriorhodopsin: counterion effects on the ^{15}N shift anisotropy. *Biochemistry.* 28:3346–3353.

Dioumaev, A. K., and M. S. Braiman. 1997. Two bathointermediates of the bacteriorhodopsin photocycle, distinguished by nanosecond time-resolved FTIR spectroscopy at room temperature. *J. Phys. Chem. B.* 101:1655–1662.

Doig, S. J., P. J. Philip, and R. A. Mathies. 1991. Picosecond time-resolved resonance Raman spectroscopy of bacteriorhodopsin's J, K, and KL intermediates. *J. Phys. Chem.* 95:6372–6379.

Dupuis, M., S. Chin, and A. Marquez. 1994. Relativistic and Electron Correlation Effects in Molecules. G. Malli, editor. Plenum Press, New York.

Dunning, T. H., Jr., and P. J. Hay. 1977. Method of Electronic Structure Theory. H. F. Shaefer, editor. Plenum Press, New York, 1–28.

Edman, K., P. Nollert, A. Royant, H. Belrhali, E. Pebay-Peyroula, J. Hajdu, R. Neutze, and E. M. Landau. 1999. High-resolution X-ray structure of an early intermediate in the bacteriorhodopsin photocycle. *Nature.* 401: 822–826.

Facciotti, M. T., S. Rouhani, F. T. Burkard, F. M. Betancourt, K. H. Downing, R. B. Rose, G. McDermott, and R. M. Glaeser. 2001. Structure of an early intermediate in the M-state phase of the bacteriorhodopsin photocycle. *Biophys. J.* 81:3442–3455.

Field, M. J., P. A. Bash, and M. Karplus. 1990. A combined quantum mechanical and molecular mechanical potential for molecular dynamics simulations. *J. Comput. Chem.* 11:700–733.

Fischer, W. B., S. Sonar, T. Marti, H. G. Khorana, and K. J. Rothschild. 1994. Detection of a water molecule in the active-site of bacteriorhodopsin: hydrogen bonding changes during the primary photoreaction. *Biochemistry.* 33:12757–12762.

Gao, J. 1997. Energy components of aqueous solution: insight from hybrid QM/MM simulations using a polarizable solvent model. *J. Comp. Chem.* 18:1062–1071.

Gao, J., and X. Xia. 1992. A priori evaluation of aqueous polarization effects through Monte Carlo QM—MM simulations. *Science.* 258: 631–635.

Garavelli, M., P. Celani, F. Bernardi, M. A. Robb, and M. Olivucci. 1997. The $C_5H_6NH_2^+$ protonated Schiff base: an *ab initio* minimal model for retinal photoisomerization. *J. Am. Chem. Soc.* 119:6891–6901.

Garavelli, M., T. Vreven, P. Celani, F. Bernardi, M. A. Robb, and M. Olivucci. 1998. Photoisomerization path for a realistic retinal chromophore model: the nonatetraenimium cation. *J. Am. Chem. Soc.* 120: 1285–1288.

Gerwert, K., B. Hess, J. Soppa, and D. Oesterhelt. 1989. Role of aspartate-96 in proton translocation by bacteriorhodopsin. *Proc. Natl. Acad. Sci. U.S.A.* 86:4943–4947.

Gogonea, V., D. Suarez, A. van der Vaart, and K. W. Merz. 2001. New developments in applying quantum mechanics to proteins. *Curr. Opin. Struct. Biol.* 11:217–223.

González-Luque, R., M. Garavelli, F. Bernardi, M. Merchán, M. A. Robb, and M. Olivucci. 2000. Computational evidence in favor of a two-state, two-mode model of the retinal chromophore photoisomerization. *Proc. Natl. Acad. Soc.* 97:9379–9384.

Grigorieff, N., T. A. Ceska, K. H. Downing, J. M. Baldwin, and R. Henderson. 1996. Electron-crystallographic refinement of the structure of bacteriorhodopsin. *J. Mol. Biol.* 259:393–421.

Hage, W., K. Munsok, H. Frei, and R. A. Mathies. 1996. Protein dynamics in the bacteriorhodopsin photocycle: a nanosecond step-scan FTIR investigation of the KL to L transition. *J. Phys. Chem.* 100:16026–16033.

Hatcher, M. E., J. G. Hu, M. Belenky, P. Verdegem, J. Lugtenburg, R. G. Griffin, and J. Herzfeld. 2002. Control of the pump cycle in bacteriorhodopsin: mechanisms elucidated by solid-state NMR of the D85N mutant. *Biophys. J.* 82:1017–1029.

Hayashi, S., and I. Ohmine. 2000. Proton transfer in bacteriorhodopsin: structure, excitation, IR spectra, and potential energy surface analyses by an ab initio QM/MM method. *J. Phys. Chem. B.* 104:10678–10691.

Hayashi, S., E. Tajkhorshid, E. Pebay-Peyroula, A. Royant, E. M. Landau, J. Navarro, and K. Schulten. 2001. Structural determinants of spectral tuning in retinal proteins-bacteriorhodopsin vs sensory rhodopsin II. *J. Phys. Chem. B.* 105:10124–10131.

Henderson, R., and P. N. T. Unwin. 1975. Three dimensional model of purple membrane obtained by electron microscopy. *Nature.* 257:28–32.

Herzfeld, J., and B. Tounge. 2000. NMR probes of vectoriality in the proton-motive photocycle of bacteriorhodopsin: evidence for an 'electrostatic steering' mechanism. *Biochim. Biophys. Acta.* 1460:95–105.

Houjou, H., Y. Inoue, and M. Sakurai. 2001. Study of the opsin shift of bacteriorhodopsin: in-sight from QM/MM calculations with electronic polarization effects of the protein environment. *J. Phys. Chem. B.* 105:867–879.

Hu, J. G., B. Q. Sun, A. T. Petkova, R. G. Griffin, and J. Herzfeld. 2001. The predischarge chromophore in bacteriorhodopsin: a ^{15}N solid-state NMR study of the L photointermediate. *Biochemistry.* 36:9316–9322.

Humphrey, W., A. Dalke, and K. Schulten. 1996. VMD-visual molecular dynamics. *J. Mol. Graph.* 14:33–38.

Humphrey, W., H. Lu, I. Logunov, H. J. Werner, and K. Schulten. 1998. Three electronic state model of the primary phototransformation of bacteriorhodopsin. *Biophys. J.* 75:1689–1699.

Kandori, H., M. Belenky, and J. Herzfeld. 2002. Vibrational frequency and dipolar orientation of the protonated Schiff base in bacteriorhodopsin before and after photoisomerization. *Biochemistry*. 41:6026–6031.

Kandori, H., N. Kinoshida, Y. Shichida, and A. Maeda. 1998a. Protein structural changes in bacteriorhodopsin upon photoisomerization as revealed by polarized FTIR spectroscopy. *J. Phys. Chem. B.* 102: 7899–7905.

Kandori, H., N. Kinoshida, Y. Shichida, A. Maeda, R. Needleman, and J. K. Lanyi. 1998b. Cysteine S—H as a hydrogen-bonding probe in proteins. *J. Am. Chem. Soc.* 120:5828–5829.

Kandori, H., N. Kinoshita, Y. Yamazaki, A. Maeda, Y. Shichida, R. Needleman, J. K. Lanyi, M. Bizounok, J. Herzfeld, J. Raap, and J. Lugtenburg. 1999. Structural change of threonine 89 upon photoisomerization in bacteriorhodopsin as revealed by polarized FTIR spectroscopy. *Biochemistry.* 38:9676–9683.

Kandori, H., N. Kinoshita, Y. Yamazaki, A. Maeda, Y. Shichida, R. Needleman, J. K. Lanyi, M. Bizounok, J. Herzfeld, J. Raap, and J. Lugtenburg. 2000. Local and distant protein structural changes on photoisomerization of the retinal in bacteriorhodopsin. *Proc. Natl. Acad. Sci. U.S.A.* 97:4643–4648.

Kandori, H., and Y. Shichida. 2000. Direct observation of the bridged water stretching vibrations inside a protein. *J. Am. Chem. Soc.* 122: 11745–11746.

Kandori, H., Y. Yamazaki, J. Sasaki, R. Needleman, J. K. Lanyi, and A. Maeda. 1995. Water-mediated proton transfer in proteins: an FTIR study of bacteriorhodopsin. *J. Am. Chem. Soc.* 117:1713–1714.

Kandori, H., Y. Yamazaki, Y. Shichida, J. Raap, J. Lugtenburg, M. Belenky, and J. Herzfeld. 2001. Tight Asp-85—Thr-89 association during the pump switch of bacteriorhodopsin. *Proc. Natl. Acad. Sci. U.S.A.* 98:1571–1576.

Kitaura, K., and K. Morokuma. 1976. A new energy decomposition scheme for molecular interactions within the Hartree-Fock approximation. *Int. J. Quantum Chem.* 10:325–340.

Logunov, I., and K. Schulten. 1996. Molecular dynamics study of the dark-adaptation process in bacteriorhodopsin. *J. Am. Chem. Soc.* 118: 9727–9737.

Lozier, R. H., R. A. Bogomolni, and W. Stoeckenius. 1975. Bacteriorhodopsin: a light-driven proton pump in *Halobacterium halobium*. *Biophys. J.* 15:955–962.

Luecke, H., H. T. Richter, and J. K. Lanyi. 1998. Proton transfer pathways in bacteriorhodopsin at 2.3 angstrom resolution. *Science*. 280: 1934–1937.

Luecke, H., B. Schobert, J. P. Cartailler, H. T. Richter, A. Rosengarth, R. Needleman, and J. K. Lanyi. 2000. Coupling photoisomerization of retinal to directional transport in bacteriorhodopsin. *J. Mol. Biol.* 300: 1237–1255.

Luecke, H., B. Schobert, J. K. Lanyi, E. N. Spudich, and J. L. Spudich. 2001. Crystal structure of sensory rhodopsin II at 2.4 Å: insights into color tuning and transducer interaction. *Science.* 293:1499–1503.

Luecke, H., B. Schobert, H. T. Richter, J. P. Cartailler, and J. K. Lanyi. 1999a. Structure of bacteriorhodopsin at 1.55 angstrom resolution. *J. Mol. Biol.* 291:899–911.

Luecke, H., B. Schobert, H. T. Richter, J. P. Cartailler, and J. K. Lanyi. 1999b. Structural changes in bacteriorhodopsin during ion transport at 2 angstrom resolution. *Science.* 286:255–261.

Maeda, A., Y. Sasaki, Y. Yamazaki, R. Needleman, and J. K. Lanyi. 1994. Interaction of aspartate-85 with a water molecule and the protonated Schiff base in the L intermediate of bacteriorhodopsin: a Fourier transform infrared spectroscopic study. *Biochemistry.* 33:1713–1717.

Maseras, M., and K. Morokuma. 1995. IMOMM: a new ab initio + molecular mechanics geometry optimization scheme of equilibrium structures and transition states. *J. Comput. Chem.* 16:1170–1179.

Merill, G. N., and M. S. Gordon. 1998. A study of small water clusters using the effective fragment potential (EFP) method. *J. Phys. Chem. A.* 102:2650–2657.

Merritt, E. A., and D. J. Bacon. 1997. Raster3D: photorealistic molecular graphics. *Method Enzymol.* 227:505–524.

Mitsuoka, K., T. Hirai, K. Murata, A. Miyazawa, A. Kidera, Y. Kimura, and Y. Fujiyoshi. 1999. The structure of bacteriorhodopsin at 3.0 Å resolution based on electron crystallography: implication of the charge distribution. *J. Mol. Biol.* 286:861–882.

Molnar, F., M. Ben-Nun, T. J. Martínez, and K. Schulten. 2000. Characterization of a conical intersection between the ground and first excited state for a retinal analog. *J. Mol. Struct. (Theochem).* 506:169–178.

Nina, M., B. Roux, and J. C. Smith. 1995. Functional interaction in bacteriorhodopsin: a theoretical analysis of retinal hydrogen bonding with water. *Biophys. J.* 68:25–39.

Oesterhelt, D., and W. Stoeckenius. 1971. Rhodopsin-like protein from the purple membrane of *Halobacterium halobium*. *Nat. New Biol.* 233: 149–152.

Pande, J., R. H. Callender, and T. G. Ebrey. 1981. Resonance Raman study of the primary photochemistry of bacteriorhodopsin. *Proc. Natl. Acad. Sci. U.S.A.* 78:7379–7382.

Pebay-Peyroula, E., R. Neutze, and E. M. Landau. 2000. Lipidic cubic phase crystallization of bacteriorhodopsin and cryotrapping of intermediates: towards resolving a resolving photocycle. *Biochim. Biophys. Acta.* 1460:119–132.

Pebay-Peyroula, E., G. Rummel, J. P. Rosenbusch, and E. M. Landau. 1997. X-ray structure of bacteriorhodopsin at 2.5 angstroms from microcrystals grown in lipidic cubic phases. *Science.* 277:1676–1681.

Rick, S. W., S. J. Stuart, and B. J. Berne. 1994. Diyamical fluctuating charge force fields: application to liquid water. *J. Chem. Phys.* 101: 453–462.

Rothschild, K. J., and H. Marrero. 1982. Infrared evidence that the Schiff base of bacteriorhodopsin is protonated: bR570 and K intermediates. *Proc. Natl. Acad. Sci. U.S.A.* 79:4045–4049.

Rothschild, K. J., P. Roepe, and J. Gillespie. 1985. Fourier transform infrared spectroscopic evidence for the existence of two conformations of the bacteriorhodopsin primary photoproduct at low temperature. *Biochim. Biophys. Acta.* 808:140–148.

Royant, A., K. Edman, T. Ursby, E. Pebay-Peyroula, E. M. Landau, and R. Neutze. 2000. Helix deformation is coupled to vectorial proton transport in the photocycle of bacteriorhodopsin. *Nature.* 406:645–648.

Royant, A., P. Nollert, K. Edman, R. Neutze, E. M. Landau, E. Pebay-Peyroula, and J. Navarro. 2001. X-ray structure of sensory rhodopsin II at 2.1 Å resolution. *Proc. Natl. Acad. Sci. U.S.A.* 98:10131–10136.

Sasaki, J., J. K. Lanyi, R. Needleman, T. Yoshizawa, and A. Maeda. 1994. Complete identification of C═O stretching vibrational bands of protonated aspartic acid residues in the difference infrared spectra of M and N intermediate versus bacteriorhodopsin. *Biochemistry.* 33:3178–3184.

Sasaki, J., A. Maeda, C. Kato, and H. Hamaguchi. 1993. Time-resolved infrared spectral analysis of the KL-to-L conversion in the photocycle of bacteriorhodopsin. *Biochemistry.* 32:867–871.

Sasaki, J., T. Yazawa, H. Kandori, A. Maeda, and H. Hamaguchi. 1995. Nanosecond time-resolved infrared spectroscopy distinguishes two K species in the bacteriorhodopsin photocycle. *Biophys. J.* 68:2073–2080.

Sass, H. J., G. Buldt, R. Gessenich, D. Hehn, D. Neff, R. Schlesinger, J. Berendzen, and P. Ormos. 2000. Structural alterations for proton translocation in the M state of wild-type bacteriorhodopsin. *Nature.* 406: 649–653.

Shichida, Y., S. Matsuoka, Y. Hidaka, and T. Yoshizawa. 1983. Absorption spectra of intermediates of bacteriorhodopsin measured by lase photolysis at room temperatures. *Biochim. Biophys. Acta.* 723:240–246.

Schulten, K., W. Humphrey, I. Logunov, M. Sheves, and D. Xu. 1995. Molecular dynamics studies of bacteriorhodopsin's photocycles. *Isr. J. Chem.* 35:447–464.

Tajkhorshid, E., J. Baudry, K. Schulten, and S. Suhai. 2000. Molecular dynamics study of the nature and origin of retinal's twisted structure in bacteriorhodopsin. *Biophys. J.* 78:683–693.

Tajkhorshid, E., B. Paizs, and S. Suhai. 1999. Role of isomerization barriers in the pK_α control of the retinal Schiff base: a density functional study. *J. Phys. Chem. B.* 103:4518–4527.

Tajkhorshid, E., and S. Suhai. 1999. Influence of the methyl groups on the structure, charge distribution, and proton affinity of the retinal Schiff base. *J. Phys. Chem. B.* 103:5581–5590.

Umeyama, H., and K. Morokuma. 1977. The origin of hydrogen bonding: an energy decomposition study. *J. Am. Chem. Soc.* 99:1316–1332.

Warshel, A., and Z. T. Chu. 2001. Nature of the surface crossing process in bacteriorhodopsin: computer simulations of the quantum dynamics of the primary photochemical event. *J. Phys. Chem. B.* 105:9857–9871.

Warshel, A., Z. T. Chu, and J.-K. Hwang. 1991. The dynamics of the primary event in rhodopsins revisited. *Chem. Phys.* 158:303–314.

Warshel, A., and M. Levitt. 1976. Theoretical studies of enzymatic reactions: dielectric, electrostatic and steric stabilization of the carbonium ion in the reaction of lysozyme. *J. Mol. Biol.* 103:227–249.

Weidlich, O., and F. Siebert. 1993. Time-resolved step-scan FT-IR investigations of the transition from KL to L in the bacteriorhodopsin photocycle: identification of chromophore twists by assigning hydrogen-out-of-plane (HOOP) bending vibrations. *Appl. Spectrosc.* 47: 1394–1400.

Xu, D., C. Martin, and K. Schulten. 1996. Molecular dynamics study of early picosecond events in the bacteriorhodopsin photocycle: dielectric response, vibrational cooling and the J, K intermediates. *Biophys. J.* 70:453–460.

Yamamoto, N., T. W. Ebbesen, and H. Ohtani. 1994. Does the KL intermediate exist in the photocycle of bacteriorhodopsin? *Chem. Phys. Lett.* 228:61–65.

Yamato, T., and T. Kakitani. 1997. Molecular dynamics simulation of the excited-state dynamics of bacteriorhodopsin. *Photochem. Photobiol.* 66: 735–740.

Zhou, F., W. Andreas, and K. Schulten. 1993. Molecular dynamics study of the proton pump cycle of bacteriorhodopsin. *Biochemistry.* 32: 2291–2306.